# Investigation of changes in Briksdalsbreen, western Norway from 1966 – 2020 using remote sensing


UNIVERSITY OF BERGEN

Faculty of Mathematics and Natural Sciences

Department of Geoscience

Master's Thesis in Geoscience

Saheed Opeyemi Adebunmi

## Abstract

Briksdalsbreen in western Norway was studied using remote sensing. Sets of optical aerial photographs captured between 1966 to 2020 were used with LiDAR-based Digital Elevation Models (DEMs) and glacier outlines derived from satellite images to estimate the changes in length, area, surface elevation and mass balance of the glacier. The results show that Briksdalsbreen retreated a total of ~ 450 m and shrunk by 0.25 $Km^2$ (0.04 % $a^{-1}$) between 1966 and 2020; however, it advanced between 1966 to 2001 before it retreated between 2001 – 2010. The glacier fronts thickened by less than ~ 0.5 m during the period of advancement in the late 90s but the total glacier thinned by ~ 3 m in the whole period of 54 years (1966 – 2020). The estimated mass balance is -0.045 m w. e. $a^{-1}$ for Briksdalsbreen between 1966 and 2020 and -0.246 m w. e. $a^{-1}$ for the period of 2010 – 2020. The result of the length estimate from this study agrees with field observation and the surface elevation change found for 2010 - 2020 conforms with the results from regional remote sensing investigation. However, the lack of published mass balance data for Briksdalsbreen and high uncertainty in comparing the mass balance of glaciers limited a comparative assessment of the estimated mass balance. Nevertheless, this study confirms that Briksdalsbreen is retreating rapidly and losing mass like many other glaciers in Norway. It also identifies increased summer temperature as the driving force of the glacier retreat since early 2000, although high winter precipitation had early caused its expansion between 1966 to 2001. The study demonstrates that remote sensing is a useful tool in glacier change assessment.

**Acknowledgement**

I am highly grateful to my supervisor, Benjamin Aubrey Robson. I benefited greatly from his vast knowledge of remote sensing and enjoyed his support throughout my studies at UiB. His kindness and patience know no bound and his responsiveness saw me through the completion of this thesis.

I say a big thank you to the Department of Geoscience, University of Bergen for the data and resources provided to me for this thesis. This gratitude is extended to UiB community at large for availing me the opportunity to be part of it.

I received some nice pictures of Briksdalsbreen from Atle Nesje. It is indeed a privilege. Thank you.

Finally, I appreciate the effort of everyone who directly and indirectly contributed to the completion of this thesis.

## Content

## List of Figures

**List of Tables**

# Chapter 1 : Introduction

This chapter presents a brief motivation, aim and objectives of the study. It also features the organization of the thesis.

## 1.1 Motivation

Glaciers are good climate indicators that contribute to freshwater supply, tourism, and hydroelectric power (HEP) generation (Cunde et al., 2016; IPCC 2019; Hiemstra et al., 2022; Vaughan et al., 2014). Several investigations have identified a global retreat of glaciers, and some have predicted the future disappearance of some small European glaciers and ice cap outlets by the end of 2100 (Beniston et al., 2018; Hugonnet et al., 2021; Zemp et al., 2019). Norwegian ice caps are particularly sensitive to mass balance fluctuation because of their area–elevation distribution (Akesson et al., 2017). According to a recent study, the outlet glaciers of the largest Ice cap in Europe, Jostedalsbreen situated in western Norway, lost 19% (110 $km^2$) of their Little Ice Age (LIA) area and 18% (14 $Km^3$) of their LIA volume until 2006 (Carrivick et al., 2022). During this period, Briksdalsbreen, a western outlet glacier of Jostedalsbreen shrunk in area by 48% and lost 34.4% of its volume (Carrivick et al., 2022).

The front of Briksdalsbreen is steep and reacts to mass balance perturbation within 4 to 5 years (Laumann & Nesje, 2009). Therefore, the glacier advances and retreats rapidly in response to climate change. For example, in the 1990s, during the 'briksdalsbre event' when the Scandinavia maritime glaciers expanded owing to mild winter precipitation associated with decadal atmospheric circulation (Nesje & Mattews, 2012), the terminus of Briksdalsbreen advanced 285 m in less than a decade during. Likewise, in the early 2000s when summer temperature increased, Briksdalsbreen retreated 145 m in a year (2005/2006), recording the maximum retreat since 1900 and a total of 486 m between 1996/1997 and 2009 (Nesje and Mattews, 2012). In the last two decades, the Briksdalsbreen terminus has retreated significantly (Figure 1.1) due to global warming. Some studies predicted that the glacier front may vanish by end of the century (Beniston et al., 2018; Laumann & Nesje, 2009). As such, regular observation, and assessment of changes on Briksdalsbreen are important.

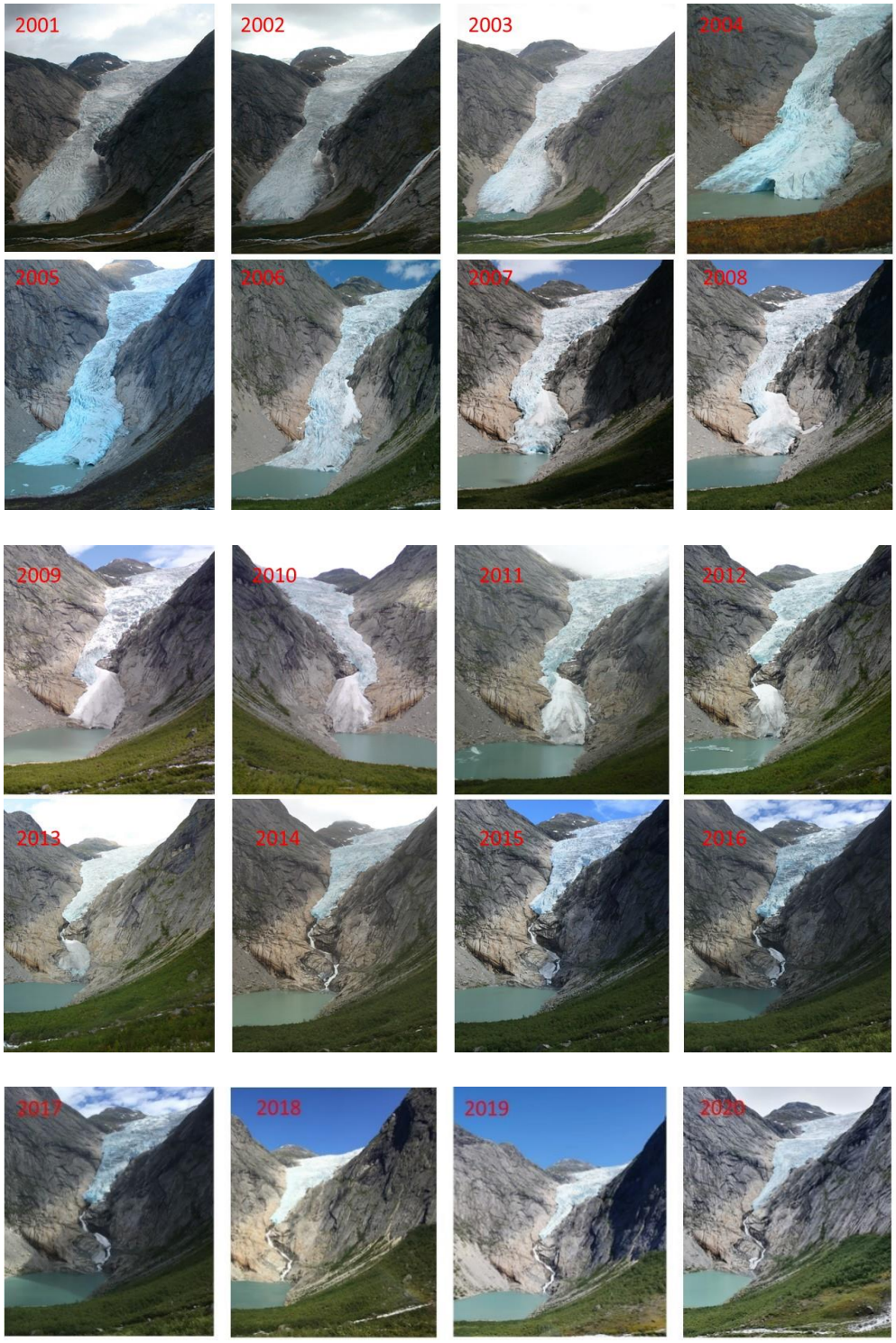


*Figure 1.1: Pictures of Briksdalsbreen terminus from 2001 to 2020. The glacier front has retreated significantly in the last two decades. The glacier head has withdrawn from lake Briksdalsvatnet and retreated up its valley to a high elevation. Courtesy: Atle Nesje, Department of Geoscience, University of Bergen, Norway*

Observational data is pertinent to understanding environmental processes, nevertheless, quality, homogenous and long-term measurements of glacier retreat are rear (Beniston et al., 2018). Regular measurement of changes in the length of Briksdalsbreen commenced in 1900 by the Norwegian Water Resources and Energy Directorate (NVE) and was continued until 2015 when the glacier front retreated to an inaccessible higher elevation (Andreasen, 2020). Some studies have used this NVE length change observation to explain the observed shrinkage and expansion of Briksdalabreen in terms of varying winter precipitation and summer temperatures (see Nesje, 2005; Nesje & Mattews, 2012) while others utilized it as a calibration tool to model the possible future changes on the glacier (see Laumann & Nesje, 2009). Nevertheless, the study of Briksdalsbreen has received little attention in recent years on the possible account of the lack of systematic observation of the surface mass balance of the glacier by the NVE (Nesje, 2005).

The high steepness and numerous crevasses of Briksdalsbreen can present challenges to field investigation of the glacier. In such a case, remote sensing offers a viable method to indirectly obtain useful information about the glacier (Paul et al, 2015; Taylor et al., 2021). Although remotely sensed data cannot absolutely substitute in situ observation, it provides an alternative way of measuring several glacier parameters such as the area, elevation change, mass balance and surface velocity. Remote sensing can be used to study glacier changes as well as infer mass balance inter-comparison of Digital Elevation models. While glacier extents can be delineated from satellite images, studies revealed that Digital Elevation Models (DEM) generated from aerial photographs with available ground control points (GCP) provide the most reliable volume change and mass balance estimates of single glaciers; likewise, high-resolution topographic information can be extracted from airborne laser scanning (Kaab et al., 2014). Unlike satellite images, aerial photographs lack extensive global ground surface coverage (Kaab et al., 2014); fortunately, some sets of aerial photographs covering Briksdalsbreen in the last 60 years are available and accessible. Despite the potential of a good temporal resolution offered by these datasets, only a few investigations have explored these resources to study Briksdalsbreen. Using recent GIS and remote sensing software to process these aerial photographs and available LiDAR data can allow a good estimation of the elevation changes and mass balance of Briksdalsbreen.

Consequently, this study is conducted to provide an update on the glaciological state of Briksdalsbreen by quantifying changes in the area, length, volume, and geodetic mass balance using remotely sensed data consisting of aerial photographs covering Briksdalsbreen between 1960 and 2020. To access the methods used in this study, results were compared with the available field observations and other relevant published results. Furthermore, an attempt was made to explain the recent changes based on the accessible representative meteorological data of the study area.

### 1.2 Aim, objectives and research questions

This study aims to investigate how Briksdalsbreen, an outlet glacier of the Jostedalsbreen ice cap in western Norway has changed between 1960 – 2020. The specific objectives of the study are listed below:

1. To estimate changes in the length, area, volume and geodetic mass balance of the glacier between 1960 and 2020
2. To compare estimated changes with in situ measurements from the area and western Norway
3. To examine the correlation between the estimated changes and the observed climatic condition within this period

These objectives are transformed into the following research questions.

i. By how much has the length, area, volume, and mass balance of Briksdalsbreen glacier changed in the last 50 years?
ii. Does the estimates from remote sensing investigation agree with situ measurements?
iii. Can the measured changes be explained by climate data?

### 1.3 Organization of the thesis

The next chapter presents a review of the relevant literature. Chapter 3 describes the geography, climate and glaciology of the study area are described. The data and methods used in this investigation are examined in chapter 4 while the results of the study are presented in chapter 5. These results are discussed in Chapter 5 and a conclusion is made in the 6$^{th}$ chapter.

## Chapter 2 : Literature Review

Glaciers are important components of the cryosphere, and their changes can be investigated through field measurement and remote sensing. Remote sensing has some advantages over field methods but is not without limitations. Both methods have been used to investigate the changes in Norwegian glaciers by measuring and observing different glacier parameters. This chapter reviews these subjects within the scope of this research and with a view to presenting a background that allows the comprehension and justification of this study.

### 2.1 Glaciers, Ice caps, outlet glaciers and zones in a glacier

Glaciers are perennial bodies of moving ice ranging in size from Greenland and Antarctica ice sheets to small mountain glaciers (Postband & Lachapelle, 2000). In the same context, ice caps are domed-shaped ice bodies that flow radially outward and often cover the underlying surface topography (Andreasson et al., 2012; Kaab et al., 2014). They can be any size but are generally smaller than ice sheets. Typical examples of ice caps in Norway are Jostedalsbreen, Folgefonna and Hardangerjøkulen. Ice caps are usually drained by outlet glaciers, a valley glacier type with a distinct front (Andreassen et al., 2012). Nigardsbreen and Briksdalsbreen are examples of outlet glaciers in Jostaldalsbreen, the largest ice cap in Norway.

A glacier can be divided into accumulation and ablation zones (Figure 2.1) with respect to changes in its mass balance (Cuffey & Paterson, 2010). Deposition of snow occurs in the accumulation zone at the high part of a glacier through snowfall, wind drift, avalanches, condensation, re-sublimation and internal accumulation. In the low ablation area, snow mass can be lost through melting, wind erosion, avalanches, sublimation and calving. Hypothetically, accumulation and

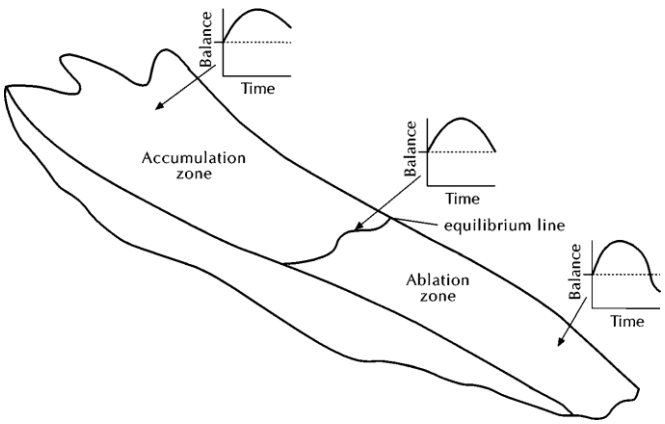


*Figure 2.1: Zones in a glacier. Mass is gained in accumulation zone and lost in the ablation zone. Both zones are separated by equilibrium line where rate of mass loss equals the mass gain (Cuffey & Paterson, 2010)*

ablation zones are separated by the equilibrium line where a balance exists between the rate of mass gain and mass loss. The annual altitude of Equilibrium Line Altitude (ELA) may vary in respect of the amount of accumulation and ablation (Cuffey & Paterson, 2010). In general, temperate glaciers lack distinct equilibrium lines, and the accumulation zone of outlet glaciers may be difficult to define (Andreassen et al., 2012).

### 2.2 Importance of glacier measurement

The cryosphere supports a significant proportion of the global population by constituting a reservoir that stores 69% (Gleick, 1996) of the world's freshwater and provides an aesthetic, cultural and recreational environment that supports tourism (Cunde et al., 2016; IPCC 2019; Viviroli et al., 2011). In addition, glaciers and snow run-off are key inputs in the development of hydroelectric power (HEP) which account for 16% of globally generated electricity (IPCC, 2019),. In Norway, 15% of the country's HEP is generated from glacier catchment (Robson, 2012). Globally, glaciers except for Antarctica, Greenland, the Canadian and Russian Arctic and Svalbard include approximately 170,000 mountain glaciers covering an area of ~250,000 $km^2$ and have a volume of 87 ± 15 mm SLE while in Scandinavia, they occupy ~2950 $km^2$ of the land area and have an estimated volume of 0.7 ± 0.2 mm SLE (Farinotti et al., 2019). However, mountain glaciers and other components of the cryosphere exhibit rapid and sustained environmental change (Beniston et al., 2018; Zemp et al., 2019).

Glaciers are sensitive to climate change (IPCC, 2019). Temperate glaciers and ice caps respond faster to climate perturbation because they maintain a temperature close to their melting point, therefore, they represent good climate indicators on the human timescale (Kaab et al., 2014; Nesje, 2005) The dynamic response of a glacier to climate change relates to how atmospheric conditions such as air temperature, precipitation, cloudiness, solar radiation and wind interact in a complex chain of processes that alter the mass and energy balance at the surface of the glacier (Kaab et al., 2014). Long-term temporal fluctuations in the mass balance of a glacier as a result of winter accumulation and summer ablation (melting) manifests as length, area, thickness and volume variation. Although measurement of mass balance can resolve the annual atmospheric conditions, changes in glacier length (or area) can provide an easy, indirect, delayed, integrated and filtered

assessment of climate change (Haeberli, 1998), thus, providing the public with the most compelling visual evidence of climate perturbation (Kaab et al., 2014).

In the last two decades (2001 – 2020), global surface temperature has increased by 0.9$^{o}$C relative to 1850 – 1900 and may likely exceed 2$^{o}$C (IPCC, 2021) under high and very high Green House Gas (GHG) emission scenarios by 2100 (Figure 2.2). This anthropogenic - driven global warming has been identified as the likely cause of global glacier retreat since the 1900 (IPCC, 2021).

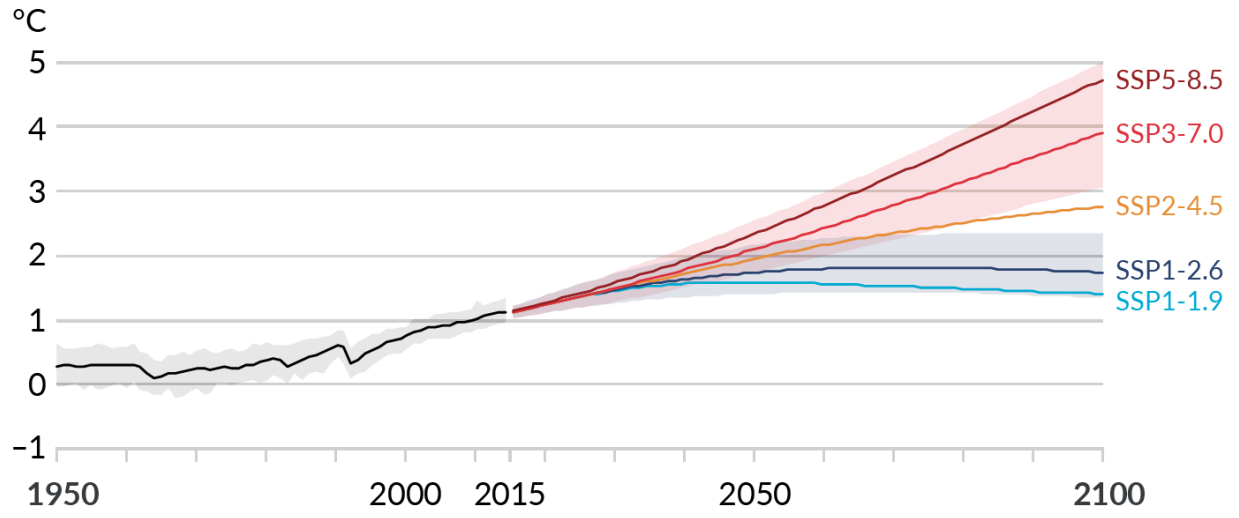


*Figure 2.2: Global surface temperature rise relative to 1850 -1900 period and Changes in global surface temperature for five illustrative emission scenarios. SSP1-1.9 and SSP1-2.6 are low and very Green House Gases (GHG) emission scenarios respectively. With SSP2-4.5 (Intermediate GHG scnerio global warming of 2oC is extremely likely to be exceed but will be exceeded in SSP2-4.5 and SSP3-7 (high and very high GHG scenarios). IPCC 2021*

Several studies have reported a global retreat, mass loss and thinning of glaciers since the little ice age. The last century witnessed an accelerated rate of glacier down casting with the melting of ~ 6.1 trillion tons of glaciers ice from 1994 to 2017 representing ~ 22% of Earth's ice loss during that period (Edwards et al., 2021). The European Alps lost an ice volume of 49% between 1900 – 2011 (Beniston et al., 2018). Although uncertainties in the projection of the future evolution of glaciers are still considerable, all models suggest that most European glaciers by 2100 may continue to experience volume reduction with a possibility of the complete disappearance of small

glaciers and tongues of many glaciers including Briksdalsbreen (Figure 2.3) whereas some large valley glaciers (such as Rhone in Switzerland) and even ice caps (such as Hardangerjokulen in Norway) may lose up to 90% of their volume (Akesson et al., 2017; Beniston et al, 2018; Laumann & Nesje, 2009).

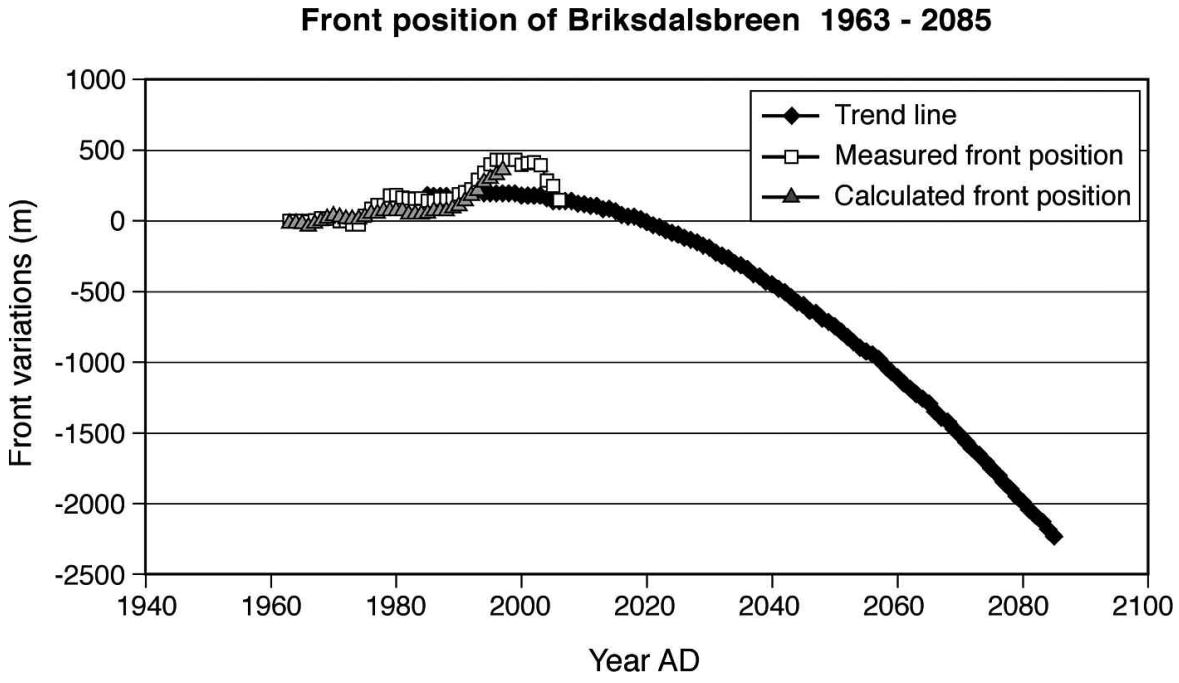


*Figure 2.3: Briksdalsbreen is projected to retreat by about 2.5 km by 2085. This includes all the glacier front. Laumann and Nesje, 2009*

Aside from the contribution of glacier melting to global sea-level rise, reduced water discharge from diminished glacier can contribute to shifts in agriculture production, less hydropower potential in summer and may result in shorter skiing seasons (Jargard et al., 2010; Kumar et al., 2011; Steiger, 2010). Glacier wasting may also increase the frequency and magnitude of cascading geohazard events such as rockfall, landslides, glacier lake outbursts, avalanches and debris flow (Haeberli et al, 2001; IPCC, 2012). An optimum adaptation strategy to mitigate these unfavourable impacts of glacier depletion can be designed from information obtained by analysing data acquired from the regular and repeated measurement of glaciers (Beniston et al., 2018). Likewise, detailed analysis of instrumental, historical and proxy data sets acquired on glaciers can be combined with glacier models to distinguish natural climate variability from human induced variability (Nesje, 2005).

## 2.3 Field measurement of glaciers in Norway

Glaciers occupy 0.7% (2692 ± 81 $Km^2$) of Norway and about 15% of the runoff from these glaciated basins contributes to hydropower production which accounts for 98% of the electricity generated in the country (Andreassen et al., 2005). Although glacier length change measurement on some Norwegian glaciers started around 1900, systematic studies of the mass balance of most Norwegian glaciers commenced in the 1960s by the glacier division of the Norwegian Water Resources and Energy Directorate (NVE) (Andreassen et al., 2020). NVE is also responsible for publishing these measurements and the results of other glaciological investigations since 1963 (Andreassen et al., 2012). In addition to studies conducted by NVE on Norwegian glaciers, individuals and other institutions have also contributed to these investigations in the form of bachelor, master's, or doctoral theses, contract work for hydropower companies, and national research projects (Andreassen et al., 2012).

An overview of glaciers with length changes and mass balance measurements can be found in NVE archives (Andreassen et al., 2020). The same in-situ methods (Figure 2.4) of snow depth probing to previous year's glaciers surface, stake reading, sounding and snow coring (for density measurement and snow depth confirmation) have been employed to measure surface (glaciological) mass balance on Norwegian glaciers over the years (Andreassen et al., 2005). Winter balance is measured in April/May while summer balance is measured in September/Octerber. A recent study identified a series of 43 Norwegian glaciers with surface mass balance records, however, only 10 of these glaciers have more than 50 years of consecutive measurements (Andreassen et al., 2020,). These long-time series glaciers are Langfjordjøkelen, Hansebreen, Austdalsbreen, seven reference glaciers including six glaciers from southern Norway (Ålfotbreen, Nigardsbreen, Rembesdalskåka, Storbreen, Hellstugubreen and Gråsubreen) representing west–east profile of maritime to continental climate and Engabreen in Northern Norway (Andreassen et al., 2020). Storbreen in Jotunheimen has the longest (73 years) continuous surface mass balance data (Andreassen & Elvehøy, 2021). To the knowledge of the author at the time of the study, no systematic record of surface mass balance has been documented for Briksdalsbreen.


*Figure 2.4 Field measurement of mass balance: (A) Stake for snow depth measurement (B) automated stake (C) snow probing, (D) snow thickness measurement with ground-penetrating radar, (E) snow pit excavation (F) snow density measurement, (G) snow coring for snow density measurement, (H) markers painted rocks to monitor snow sutface changes (Nivometer)). Geibel et al, 2022; Photos: M. Huss (A, E-G), C. Ogier (B-D), P. L. Mercanton (H).*

Direct length change observations on Norwegian glaciers are made by measuring the distance between the glacier terminus and fixed reference point on an annual or multi-annual base (Andreassen et al., 2005). Records of length changes of about 49 glaciers are available from the 1960s and onward, but measurements of 10 of these glaciers have been discontinued by 2018 (Andreassen et al., 2020). Measurement of changes in the length of glaciers such as Briksdalsbreen, Bødalsbreen, Bøyabreen, Store Supphellebreen, kjenndalsbreen and Bergsetbreen have been terminated in 2015, 2015, 2014, 2014, 2009, 2006 respectively because their termini were no longer accessible (Andreassen et al., 2020,). In the early days of ice thickness measurement in Norway (1960), markers inscribed on rocks (Figure 4), hot water drilling and seismic sounding were used on selected glaciers e.g., Rembedalskåha and Folgefonna, however,

ground penetrating radar which has become a favourable method from 1980 until today has been used to access the thickness of ice on Jostedalsbreen (Andreassen et al., 2012). On ice cap outlets with heavy crevasses such as Hardangerjøkulen, radio–echo measurement has been conducted from a helicopter (Melvold et al., 2011). Other investigations like glacier dynamics involving the measurement of the surface velocity of glaciers from a repeated survey of stakes have been carried out on Austerdalsbreen since 1987 (Andreassen et al., 2021). However, it is unlikely that these methods have been used on Briksdalsbreen as in-situ thickness and glacier velocity data of the glaciers have not been properly documented.

### 2.4 Application of Remote Sensing in Glaciology

In glaciology, remote sensing exploits the variability of the properties of glacier components such as ice, firn, snow, water, rocks and debris in the different electromagnetic spectrums (natural or instrument generated) to provide information about them from a distance. Optical remote sensing uses visible and near-infrared (VNIR) regions of the electromagnetic spectrum which range from 0.4 to 2.5 μm and optical data with medium to high spatial resolution such as images from Landsat TM, ETM+ and ASTER sensors are regularly employed to monitor and map glaciers with exceeding application in temporal change analysis of the spatial extent of snow and glaciers area (Way et al, 2014; Kaab et al., 2014; Pfeffer et al., 2014). In addition, optical photogrammetry enables the processing of aerial photographs and satellite images of glaciers into surface elevation information in the form of Digital elevation models (DEM) which is useful in the assessment of changes in glacier thickness, volume and mass balance (Paul et al., 2012). Consequently, optical remote sensing can provide information on the topography and geometry of glaciers. Remote sensing applied in the thermal band (8 – 14 μm) can resolve debris cover on glaciers and microwave remote sensing is often applied to map glacier facies and study snow properties such as snow water equivalent (SWE), snow wetness and snow depth (Konig, 2001). With the development of Light detection and ranging (LiDAR) scanning and interferometric synthetic aperture (InSAR) technologies such as Shuttle Radar Topography Mission (SRTM) and TanDEM-X which measure changes on glacier surfaces using the phase difference between two returned signals, highly accurate DEM can be created, and estimation of glacier velocity became possible (Kaab et al., 2014). In a holistic sense, applying remote sensing in different bands of

electromagnetic radiation can allow the investigation of the dynamics and evolution of glaciers. Furthermore, the increasingly popular use of Unmanned Aerial Vehicles (UAV) and drones based remote sensing, upcoming satellite missions coupled with Artificial intelligence/Machine Learning-based image processing techniques promise a better understanding of glaciers with remote sensing in the nearest future (Hoeser and Kuenzer; 2020; Taylor et al., 2021; Zhu et al., 2017).

### 2.5 Advantages and disadvantages of remote sensing over field methods

Remotely sensed data are used to complement field measurements, especially on glaciers with poor accessibility and large extent (Paul et al., 2015). Only ~2.5 % of the world's glacier is measured on the field (WGMS, 2016) as most of the world's glaciers exist in remote, rugged and hostile environments while field investigation of some glaciers is limited by legislation (Gudmundsson et al., 2011; Kääb et al., 2005b; Taylor et al., 2021). The financial, logistic, and time-related challenges associated with the collection of in-situ data in these areas can be circumvented by employing remote sensing to obtain useful information. Moreover, monitoring and mapping glaciers on a regional and global scale as well as the creation of glacier inventory (e.g., World Glacier Inventory and Randolph Glacier inventory) have relied on the availability of advanced high-resolution satellite data (Baumann et al., 2021). Furthermore, remote sensing enables the observation of glaciological records at a higher frequency and temporal resolution due to the low period of satellite image acquisition and the availability of archives of old aerial photos that allows the extension of glacier observations further back in time (Paul et al., 2015; Taylor et al., 2021).

Remote sensing suffers limitations related to spatial resolution, errors of spatial similarity, weather conditions and failure to measure mass balance directly (Robson, 2012). Features smaller than the size of the pixel of an image cannot be resolved and the different surfaces within the same pixel can be wrongly assigned to a particular landform, therefore, expensive high-resolution images are needed to study small glaciers (Kääb, 2002; Konig et al., 2001; Robson, 2012). Likewise, features (e.g., glacier ice and cloud) with similar spectral signatures can be misinterpreted (Andreassen et al., 2008) thereby adding to the uncertainty in the results. Furthermore, a major drawback of optical remote sensing is its limitation to daylight and cloud-free condition which can be hardly avoided

in the physical settings of mountain glaciers (Andreassen et al., 2008; Racoviteanu et al., 2008). Important areas of interest can be masked by shadows due to complex topography and high relief (Robson, 2012). Although radar sensors can penetrate clouds, it is affected by radar shadow and layover from steep slopes and signal decorrelation related to a highly dynamic environment (Taylor et al., 2021). In contrast to glaciological mass balance, geodetic mass balance includes internal and basal balances, however, no remote sensing method can measure this important barometer of glacier's health directly (Robson, 2012).

### 2.6 Remotely sensed glaciers parameters

Remote sensing can measure various glacier variables; however, this study utilized the method to estimate changes in glacier length, area, volume and geodetic mass balance. Several studies have also employed the remote sensing to measure glacier surface velocity and map glacier facies (see Robson et al., 2022; Zhang et al., 2019).

#### 2.6.1 Glacier area and length change

Glacier area is commonly obtained by manual delineation of glaciers from satellite images acquired at the end of ablation season. However, band ratioing has been proven to be efficient and robust at automatically delineating clean glacier ice with accuracies > 95% (Robson et al., 2015). The band ratios method works by contrasting the response of glaciers in visible and Short-Wave Infrared (SWIR) regions such that the high reflectance of glaciers in the Visible and Near Infrared (VNIR) region is divided by the low reflectance of glaciers in the SWIR region to get a high-value result. Possible band rationing includes TM3 and TM5 (RED/SWIR), TM4 or TM5 (NIR/SWIR), or the natural difference snow index (NDSI) and threshold can apply to separate glaciers found the background soil, rock and vegetation (Andreassen et al., 2008). Figure 2.5 shows an illustration of automated band rationing applied in the classification of glaciers in Jotunheimen by Andreassen et al. (2012) using Landsat TM images. Although complete glacier delineations were not performed in this study, ready-made outlines of Briksdalsbreen and its catchment were downloaded and used.

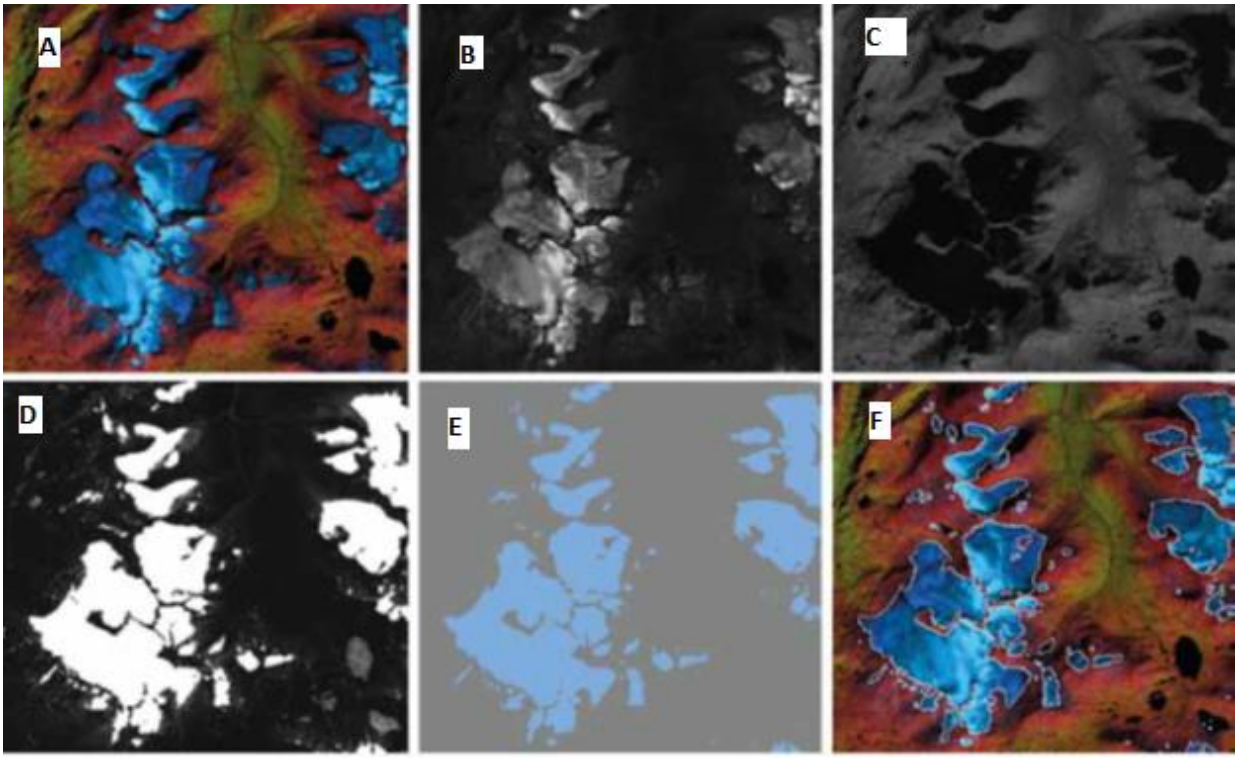


*Figure 2.5: Band rationing delineation of Jotunheimen glaciers using a Landsat TM scene from 9 August 2003. (A) Red-green-blue (RGB) composite of TM bands 5, 4 and 3, (B) Landsat band TM3, (C) Landsat band TM5 (NIR), (D) ratio image of TM3/TM5, (E) thresholded image of TM3/TM5 >2.0 and a median filter (3*3 kernel) applied, and F) as A) with outlines (in white) derived from raster to vector conversion of e). Andreassen et al., 2012*

Andreassen *et al*. (2020) estimated the change in length of some glaciers in Jotunheimen by measuring the distance between the elevation maps-based glacier outlines of the terminus along automatically generated flowlines (Figure 2.6).

### 2.6.2 Glacier elevation change, volume and mass balance

Glaciers thin and thicken in response to climate change. Most estimations of glacier thickness involve the measurement of changes in the surface elevation of glaciers derived by differencing two DEMs of different times. The volume difference is the summation of the vertical difference of two or more complete DEMs, otherwise, for incomplete DEMs, either the mean thickness change for each elevation bin is multiplied by its area and all bins summed (hypsographic method)

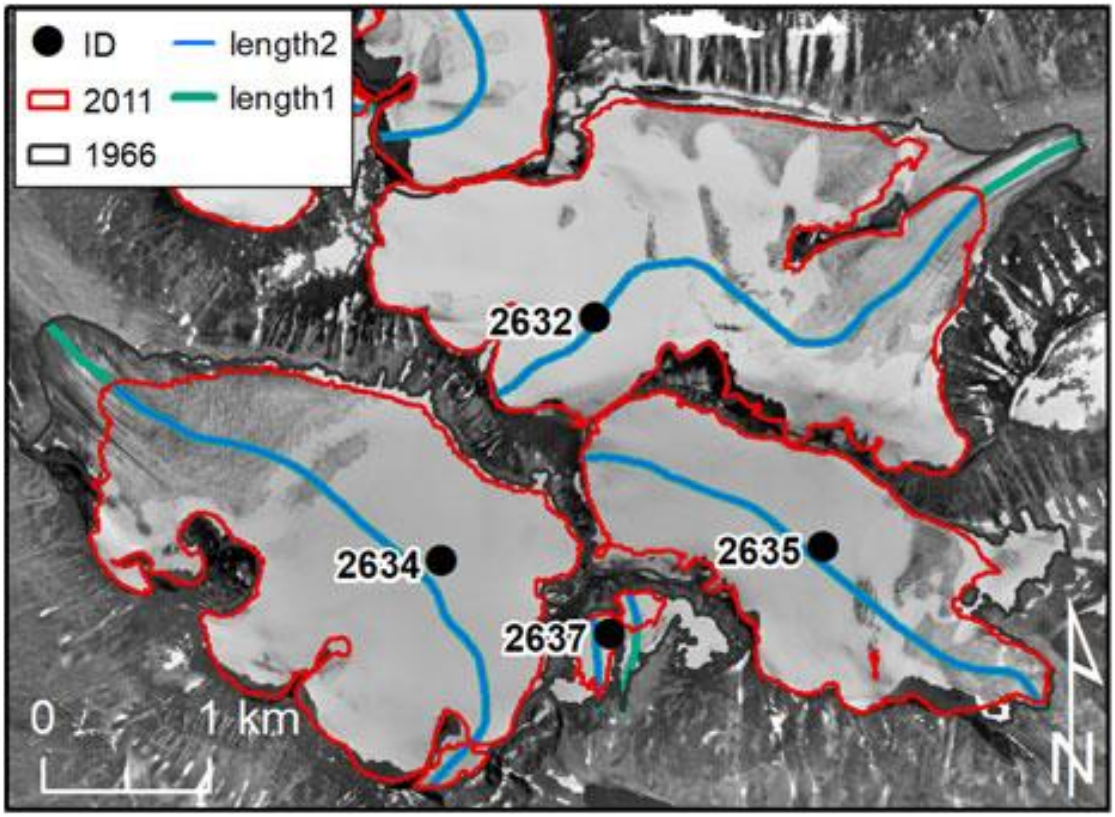


*Figure 2.6; Measurement of glacier length change from glacier outlines and flowlines on some glaciers in Jotunheimen. The difference between the intersections of the terminus outlines and the flowlines (Length 1 and length 2) glacier length change. Andreassen et al., 2020.*

or the polynomial variation of elevation changes with height can be fitted to measured elevation differences and the elevation differences for each glacier point then computed according to its height using the polynomial parameters (Kääb et al., 2014)

DEMs have been generated using photogrammetry on optical images, interferometry on microwave images and LiDAR scanning (Paul et al, 2015; Hugonnet et al., 2022). DEMs made from aerial photos provide the most reliable estimate of volume changes of single glaciers with RMS accuracies in the size of approximately one pixel (few tens of centimetres) if precise GCPs are available (Kääb, 2002), however, only little fraction of the ground surface has been covered by aerial photos. Conversely, satellite derived DEMs (e.g., ASTER DEM) can offer a regional elevation change study of glaciers if the signal and comprehensive errors are handled with caution. Airborne laser scanning systems can provide high-resolution topographic information and LiDAR

data are used as accurate ground control for photogrammetric DEM extraction (Kääb et al., 2014). Poor accuracies in DEM that manifest as elevation biases related to erroneous horizontal referencing, tilts, and vertical shifts have been minimized by methods performing three-dimensional alignment of DEMs (Hugonnet et al., 2022).

Elevation change data is an important component of glacier geodetic mass balance calculations. Volume change estimated from elevation change data can be converted to mass balance provided density information of snow is available. Density is often assumed to be constant according to Sorge's law which states that 'the density of snow at a given depth below the surface is constant'. However, while a density of 900 Kg m-3 is generally used for the ablation zone, suitable density in the accumulation zone is still a subject of research (Kääb et al., 2014). Despite this limitation, several studies have used this method to estimate geodetic mass balance, and some have found a good agreement between geodetic and glaciological mass balance (Andreassen et al.,2002; Zemp et al. 2010). Andreassone et al., (2020) found a mean of -0.27 m w. e. $a^{-1}$ for both geodetic and glaciological mass balance for glacier in Norway for an approximate period of 60 years.

### 2.7 Remote sensing investigation of Norwegian glaciers

Observation of Norwegian glaciers using photogrammetry on optical images dates to the 1930s when part of the Folgefonna ice cap appeared in a photograph and since then aerial photographs and satellite images (since the 1970s) of many glaciers in Norway have been systematically and repeatedly used to estimate changes in the glacier areas, volumes, elevations and (geodetic) mass balance (Andreassenet et al, 2012). For example, Andreassen et al (2002) used aerials photographs to calculate the mass balance 7 glaciers (3 in the north, 4 in the south) in Norway for a period between 1960 – 1990. Uncertainties introduced by snow-covered parts of glaciers due to poor optical contrast when generating elevation products from these images has been significantly minimized using annual data from laser scanning which is available for all mass balance glaciers and some other glaciers in Norway since 2007; consequently, the refinement of direct measurements and calibration of several glaciological mass balance series have become possible (Andreassen et al., 2012).

DTMs created from LIDAR data (2007 – 2013) and contour maps made from vertical aerial photographs from the 1960s have been used to compute the geodetic mass balance of glaciers in

Norway from the 1960s to 2018 (Andreassen et al., 2020). Likewise, many independent investigations of the thickness, volume and geodetic mass balance of selected Norwegian glaciers based on DEMs processed from old and new optical images, images and LIDAR scanning have been conducted. In the preparation of the Norwegian glacier inventory, scenes from Landsat images have been processed to delineate glaciers, map their outlines and compute their extents (Andreassen et al., 2012). Although the application of remote sensing in glaciological studies has lately gained popularity in Norway, this study is probably one of the few (if any) to employ remote sensing as a tool for investigating changes on Briksdalsbreen.

### 2.8 Past, recent and future changes of Norway glaciers

Most Norwegian glacier reached their little ice age (AD 1400 – 1850) maximum during the mid-18$^{th}$ century (Groove, 2004) with rapid advancement of glaciers of the southern glaciers in the early 18$^{th}$ century due to low summer temperature and mild winter associated with positive NAO (Nesje et al., 2008). During the 20$^{th}$ century, mainland Norwegian glaciers generally retreated with periodic advancement while outlet glaciers advanced until 1910 – 1930. All Norwegian glaciers began an obvious retreat in the 1930s due to Early 20$^{th}$ Century Warming (Andreassen et al., 2012). In the period of 1962 to 2000, while continental glaciers experience frontal retreat due to negative mass balance attributed to small summer and winter balance, most maritime glaciers experienced a surplus mass balance and advancement (Andreassen et al., 2012). Since 2000, Norwegian glaciers have thinned and retreated significantly but recorded positive mass balance in some years (2012,2014 and 2015) when NAO was positive (Andreassen et al., 2020). In a span of 50 years (1960 – 2018), the volume of Norwegian glaciers has reduced by 10% with a net glaciological mass balance of - 0.27 m w.e. $a^{-1}$ (Andreassen et al., 2020).

# Chapter 3 : Study area

This chapter describes the geography, climate and glaciology of Briksdalsbreen. It features the climatic characteristics and history of Briksdalsbreen as a maritime glacier and the impact of the North Atlantic Oscillation on its mass balance. An account of the changes in the frontal part of the glacier since the little ice age is also given.

## 3.1 Geography

Briksdalsbreen (Figure 3.1) is a steep and short valley glacier from Jostedalsbreen western Norway, the largest ice cap in Europe. It lies on the western side of the ice cap and covers an area of 11.46 $km^2$ (NVE) in 2019. The glacier spans a length of 6 km in 1988 when it ranges in altitude from 349 m – 1917 m (Nesje, 2005) but have retreated by ~ 0.5 km by 2015 (NVE). Briksdalsbreen is bordered to the east and west by Brenndalsbreen and Tjøtabree respectively while Bakilbreen, Bergsetbreen, and Nigardsbreen, a relatively well studied outlet glacier of Jostedalsbreen with a long annual mass balance record lie on its opposite side. The glacier front ends in a proglacier lake, Briksdalsvatnet. Although Briksdalsbreen has a clear and debris free surface, zones of crevasses running west - east exist near the central flowline (Rose et al., 2009). Briksdalbreen is underlain by unlithified sediments deposited on a Precambrian bedrock. Olden village, a major tourist area in the municipality of Stryn, vestland, Norway is 25 km (30 minutes' drive) north of Briksdalsbreen along the Oldendalen valley. Briksdalbreen serves recreational purpose mainly as a hiking destination for tourists and the inhabitants of the valley.

## 3.2 Climate

Western Norway, the regional domain of Briksdalsbreen has a maritime climate characterised by small annual temperature variation and high precipitation (snowfall) provided by the humid and mild south-westerly winds from the North Atlantic (Andreassen, 2012; Imhof et al., 2011). Frontal and orographic precipitation is more common in this area and occur mostly during autumn and winter. During this cold period (November – April), this region is also influenced by

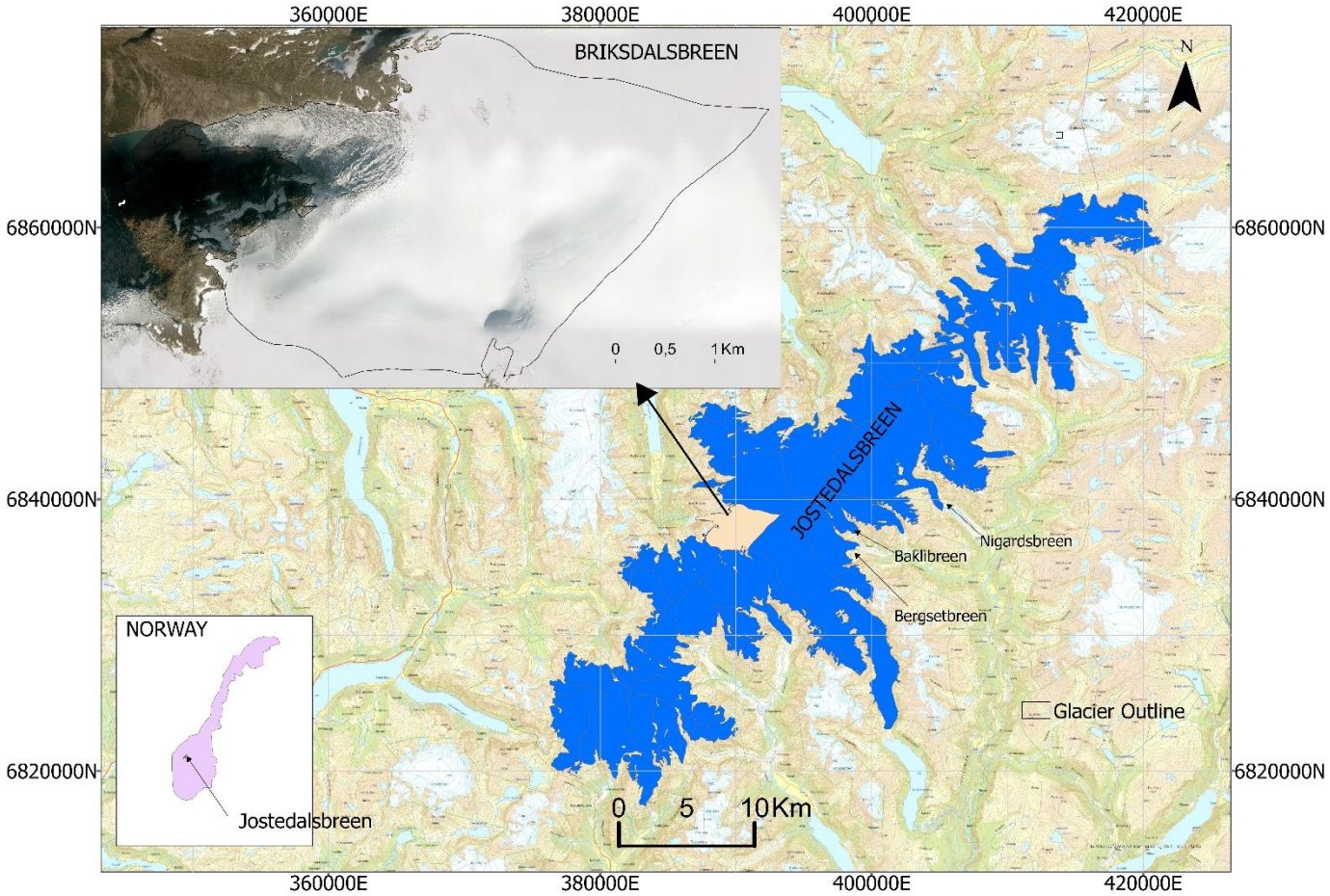


*Figure 3.1 Location of the study area. Briksdalsbreen is located on the western side of Jostedalsbreen Ice cap in Norway.*

a prominent and recurrent pattern of atmospheric variability, North Atlantic Oscillation (NAO) (Hurrell, 2003).

North Atlantic Oscillation (NAO) refers to a redistribution of atmospheric mass between Iceland and the Azores arising from pressure difference between the zones (Hurrell, 2003; Nesje, 2005). It swings from one phase to another to produce large changes in the strength of the westerly winds across the Atlantic. Positive NAO relates to mild and humid winter weather in southwestern Norway (Nesje, 2005). On contrary, Negative NAO indicates a less winter accumulation than the positive phase. NAO indices exhibit interannual and decadal trends that correlate with glacier mass balance variations observed in the late $20^{th}$ /early $21^{st}$ century in western Norway and accounts for 59% and 50% in winter balance of Ålfotbreen and Nigardsbreen respectively during a period of 1962 – 2003 (Nesje, 2005).

The mean annual temperature in western Norway is about 2100 mm with monthly precipitation greater than 200 mm (Figure 3.2) in winter and about 100 mm in summer while the mean annual temperature is about $2^{o}$ C and the average monthly temperature can be as high as $12^{o}$ C in mid-summer (July) (Figure 3.3) (Norwagian Meteriological Institute (NMI)). Based on records from Bergen and Briksdal meteorological stations (Nesje, 1995, Nesje 2005), the mean annual temperature and precipitation in Briksdalsbreen for a period of 1961 – 1990 (1961 – 1990 normal) are $12.5^{0}$C and 887 mm respectively. Summer temperature between 1901 and 1930 was below the 1961 – 1990 normal whereas it was higher between 1940 and 1950 when the highest summer temperature ($14.7^{o}$ C) of the $20^{th}$ century was documented. From the early 1950s to 1997, summer temperature fluctuated about the 1961 – 1990 normal but have shown an increasing trend till date. Winter precipitation between 1901 to 1920 was above the 1961 - 1990 normal. Between 1930 - 1960, the winter precipitation fluctuates about the normal but decreased below it in the period of 1960 - 1970. Precipitation increased after 1980 and peak around 1992. It decreased until 2000 and since then it has maintained a very low increase rate (see section 6.4).

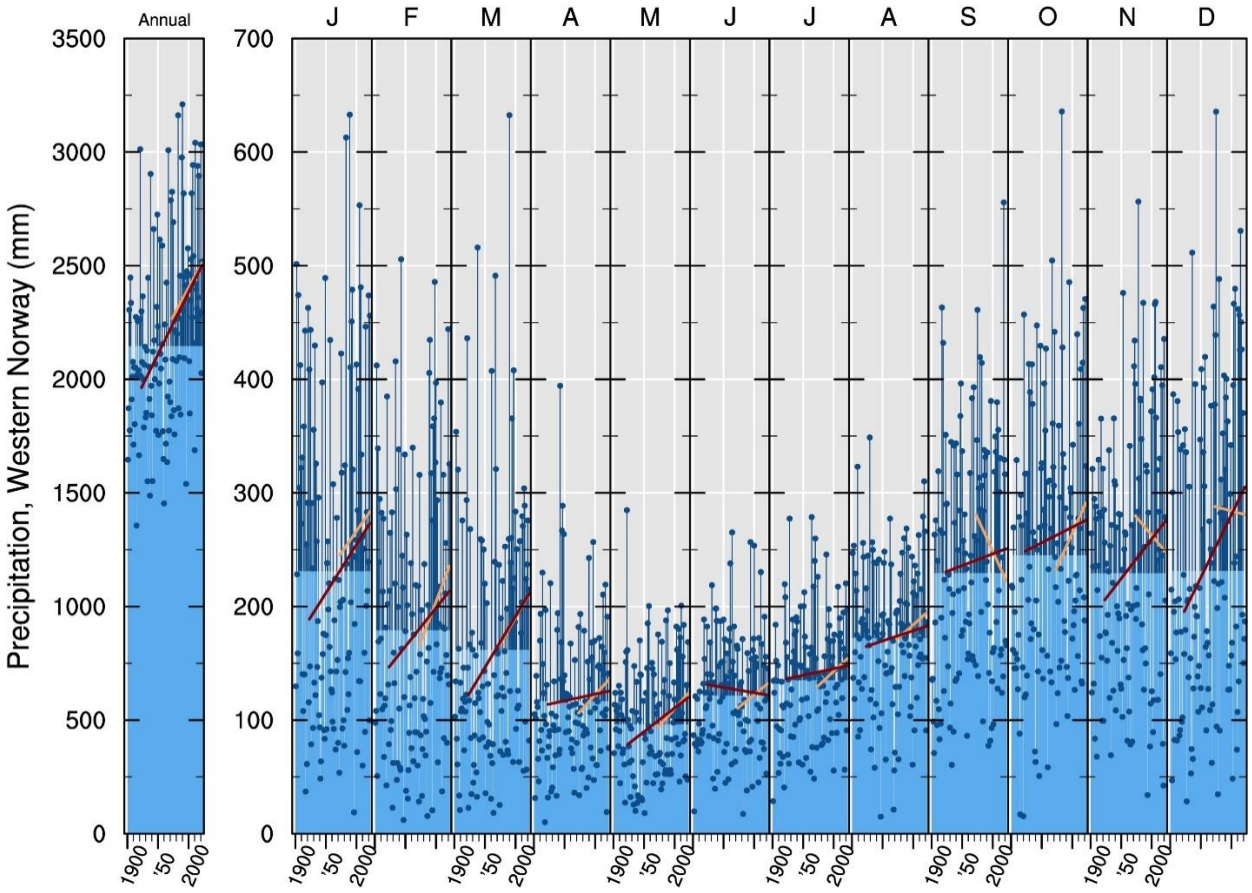


*Figure 3.2: the annual mean precipitation (left column) for western Norway and for the individual months of the year. The black and blue lines are the linear trends for the last 100 and 50 years, respectively. (downloaded from Helge Drange page: folk.uib.no/ngfhd/Climate/climate-pnor03.html).Data is eklima of Norwagian Meterological Institute.*

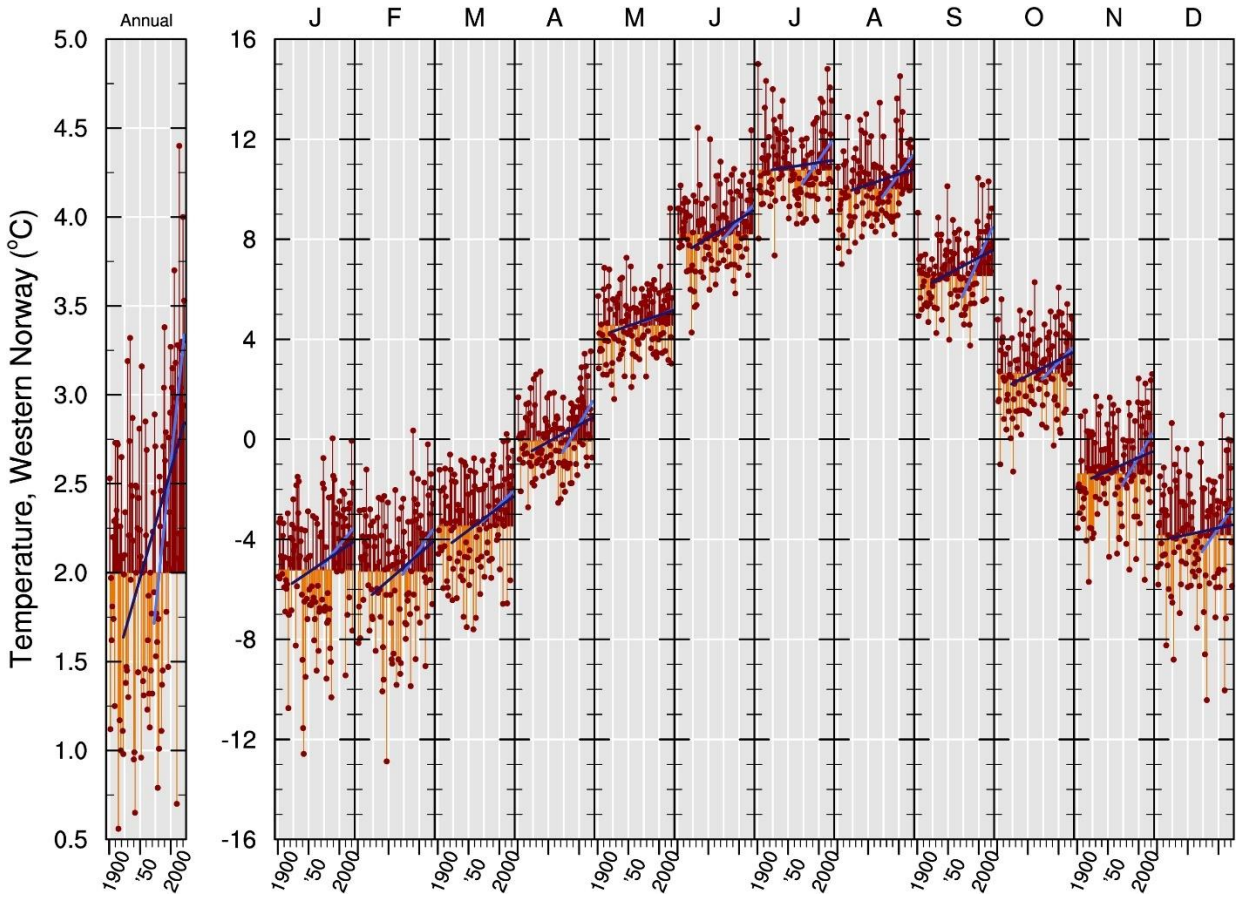


*Figure 3.3: the annual mean temperature (left column) for western Norway and for the individual months of the year. The black and blue lines are the linear trends for the last 100 and 50 years, respectively. (downloaded from Helge Drange page: folk.uib.no/ngfhd/Climate/climate-pnor03.html) Data is from frost of Norwagian Meterological institute.*

### 3.3 Previous studies on Briksdalsbreen

Nesje (1995, 2005) investigated the frontal variation of Briksdalsbreen between 1901 – 2005 based on NVE field measurement of the length changes. The glacier slightly advanced (appx 50 m) in the first decade of the 1900s because summer temperatures were low. The next decade witnessed a retreat phase until 1921 and in 1931 the glacier was 53 m behind its 1900 frontal position. Briksdalsbreen was at its 20$^{th}$-century minimum between 1932 and 1955 with the maximum annual retreat of 48 m in 1948. A combination of high summer temperatures and low winter accumulation accounted for this retreat. A high winter precipitation resulted in an advance of 278 m between 1956 – 1992. NAO positive mode amplified the advancement of the glacier in the four years that followed (1992/1993 – 1996/97). It advanced as much as 278 m during this period and was flowing outward at a mean rate of appx 22 cm/day in 1994. Between 1997 and 2004. Briksdalsbreen retreated 230 m with the largest annual retreat of 130 m in 2003/2004 on the account of high summer temperature (ablation).

Using statistical analysis of the glacier - front data a frontal time - lag of 3 – 5 years was found for the glacier (Nesje et al., 1995; Nesje 2005; L|aumann and Nesje, 2009). This value was confirmed by Laumann and Nesje (2009). In addition, Laumann and Nesje (2009) reported a response time of ~ 52 years and ~ 60 years for a mass balance perturbation of 0.3 m. w. e. an 0.6 m. w. e respectively and projected 2.5 – 5.0 km retreat of Briksdalsbreen by 2085 based on the measured mass balance between 1963 – 2007.

# Chapter 4 : Data and Methods

This chapter presents the datasets and remote sensing methods utilized in this study.

## **4.1** Data

The important raw datasets for this study are historical aerial photographs, however, glacier outlines, climate data, NVE length observation dataset, prepared aerial photograph-based DEM and LiDAR-based DEM are useful additional data.

### 4.1.1 Aerial Photographs

Aerial photogrammetry is an invaluable mapping technique that has enjoyed tremendous development in instruments and techniques. A major progress in the 21$^{st}$ century is the replacement of film-based aerial mapping cameras with high-resolution digital sensors. The land mapping division of the Norwegian Mapping Authority, Kartverket manages the historical mapping and aerial photography materials in Norway, therefore, analogue and digital aerial photographs covering Norway can be accessed from Kartverket's vast archive of historical images. For this study, 3 sets (1984, 1993, 2001) of well-scanned analogue aerial photographs and two sets (2010 and 2017) of RGB digital aerial photographs covering Briksdalsbreen with their calibration reports were generously provided by the Department of Geoscience, University of Bergen, Norway.

#### 4.1.1.1 Scanned Analogue aerial photographs.

Inspection of provided scanned analogue aerial photographs and calibration reports revealed that all the photographs were taken with single-lens frame cameras reputed for the highest geometric picture quality among the different types of traditional(analogue) imaging devices. Frame cameras acquire images simultaneously over the entire format (film) by employing shutters that open and allow light from the field of view to illuminate a two-dimensional image plane before closing. Based on the angular field of view, single-lens frame cameras are classified as normal angle ($\leq 75^{o}$), wide-angle ($75^{o}$ - $100^{o}$) and super wide angle ($> 100^{o}$).

The 2001 photographs were captured with the RC30 camera by Swissoptic AG while the 1993 photographs were taken with the RMK Top 15 (Figure 4.1) camera by Fjellanger Wideroe AS.

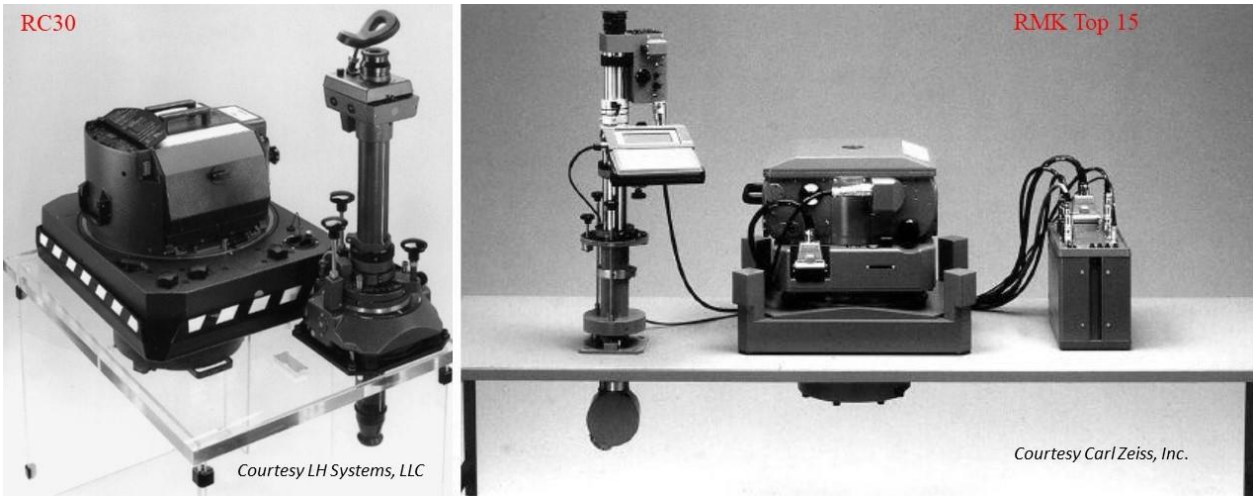


*Figure 4.1: Analogue single-lens frame photogrammetry cameras. RC30 was used for capturing 2001 and RMK Top 15 used for taking 1993 images.*

These cameras are high-precision single-lens frame mapping cameras with high film capacities (appx 500 exposures), lenses of focal length 152 mm, 230 mm square formats and provide a wide-angle field of view (98º). The predecessors of these mapping cameras, RC5, RC8, RC10 and RMK A 15/23 also produced useful photographs in the mid and late 1900s and were used to take 1960, 1967, 1984 and 1986 sets of aerial photographs respectively. Only the 1960 photograph has a 180 mm square format, others maintain 230 mm square formats with a wide-angle field of view.

All the photograph sets lack either enough coverage or the number of photographs to obtain information about the entire glacier, however, they sufficiently capture the front part of the glacier. Some images from 1960, 1967, 1997 and 1984 were also available but were not utilized. The 1997 aerial photographs were not used because they only cover the upper part of the glacier front. Likewise, photographs from 1967 were also abandoned due to a lack of sufficient overlap with others. Both 1960 and 1984 contain shadows and their produce poor DEMs and the calibration report for the 1960 aerial photograph set is missing information about the lens distortions, principal points, and fiducial marks. Only the photographs from 2001 and 1986 were scanned at the same resolution, others contain subsets scanned at slightly different resolutions. For example, the 1993 photograph sets consist of 7 photographs in total, 6 photographs with a resolution of 19680 ×

20715 and one photograph scanned at 19810 × 20689 resolution. In the 1984 and 1993 datasets, some areas in the lower part of the studied glacier front are covered by shadow. Table 4.1 presents a summary of the sets of aerial photographs used in this study while Figure 4.2 shows a photograph of an image from each set.

#### 4.1.1.2 Digital Aerial Photographs

Both the 2010 and 2017 RGB images were acquired with UltraCam photogrammetric digital-frame aerial camera. Unlike traditional frame cameras, digital-frame cameras record reflected electromagnetic energy with a 2-dimensional array of the solid-state detector elements such as charged coupled device (CCD) elements which build up electric current in proportion to the incident light at each pixel location, thus producing a digital image. Digital mapping cameras can have different formats and focal lengths; however, most are designed to capture images in the normal angle ($\leq 75^{o}$) range—narrower than those of the 152-mm focal length film camera.

The 2017 photographs were taken with a 450 Megapixel normal-angle UltraCam Eagle digital aerial photogrammetry camera (Figure 4.3) with 68.016 mm (long-track) × 104.052 mm (cross-track) image format and a resolution of 4360 pixels × 6670 pixels whereas the 2010 photographs were taken with 196 Megapixel wide-angle UltraCam Xp (Figure xxx) with 67.860 mm (long-track) × 103.860 mm (cross-track) image format and a resolution of 11310 pixels × 17310 pixels.

A summary of the information on the 2010 and 2017 digital photographs are given in Table 4.2. The 18 and 136 digital (RGB) images from the 2010 and 2017 sets respectively cover the entire catchment of Briksdalsbreen and show the lower part of the glacier front in a faint shadow. Selected images showing the glacier front of Briksdalsbreen from the 2010 and 2017 sets of photographs are shown in Figure 4.4

### 4.1.2 Additional Data

The other sets of data used in this study are glacier outlines, climate data, NVE glacier length data, prepared aerial photograph-based DEM and LiDAR-based DEM.

*Table 4.1:Information about the historical analogue photograph used in this study.*

| Date | Taken by | Camera Type | Scale | CLF(mm) |
|---|---|---|---|---|
| 1984 | Fjellanger Wideroe AS | RC10 | 1:50000 | 152.99 |
| 1993 | Fjellanger Wideroe AS | RMK Top 15 camera | 1:50000 | 153.64 |
| 2001 | Swissoptic AG | RC30 | 1:15000 | 153.34 |

*Table 4.2: Source, instrument, resolution and focal length of the digital images used in this study.*

| Date | Taken by | Camera type | Pixel size (µm) | Focal lenght (mm) |
|---|---|---|---|---|
| 2010 | Blom Geomatics AS | UltraCam Xp | 6.0 | 100.5 |
| 2017 | TerraTec As | UltaCam Eagle | 5.2 | 100.5 |

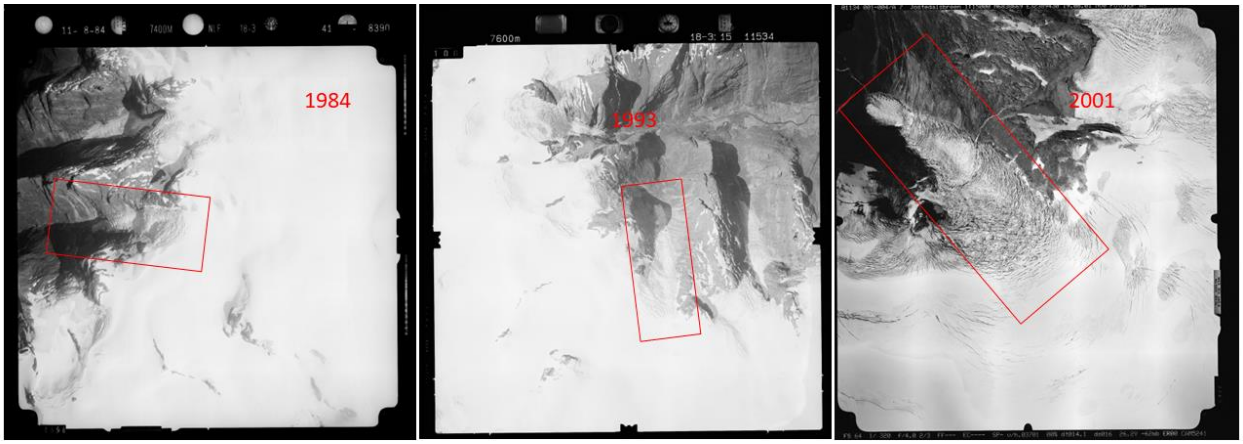


*Figure 4.2: Sample scenes from each set of analogue aerial photographs. The red box shows the study glacier front.*


*Figure 4.3: UltraCam photogrammetric digital-frame aerial camera. 2010 images were taken with Ultracam Xp while 2017 images were captured with UltraCam Eagle. (www.vexcel-imaging.com)*

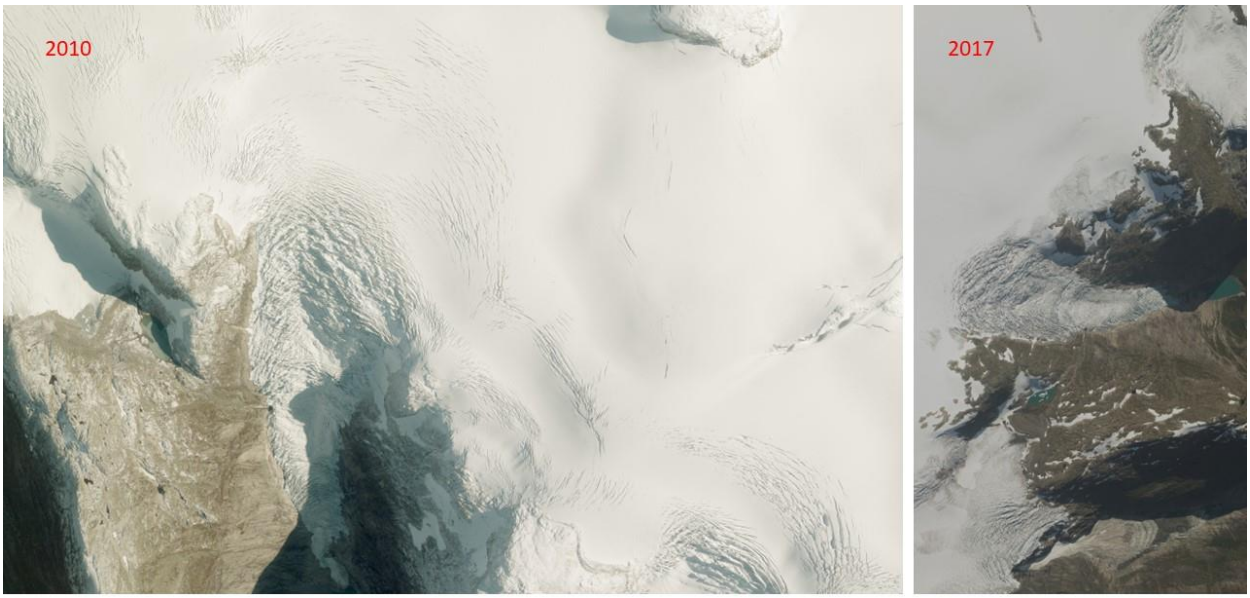


*Figure 4.4: Sample images from the 2010 and 2017 digital aerial photograph.*

#### 4.1.2.1 Glacier Outlines

Glacier outlines were needed to process the aerial photographs and determine the area and length change of the glacier. Three sets of glacier area outlines covering the period 1988-1997, 1996-2006, and 2018-2019 for mainland Norway including Briksdalsbreen were downloaded from the NVE's website. Both the 1988-1997 and 1996 -2006 outlines were delineated from Landsat TM/ETM+ satellite images (Andreassen et al.,2012) at 30 m resolution while 2018-2019 was based on Sentinel-2 images at 10 m resolution (Andreassen et al., 2022). In addition, the 1966 outline of the Jostedalsbreen Ice cap and its outlet glaciers was graciously provided by Benjamin Robson of the Department of Geoscience, University of Bergen, Norway. All glacier outline datasets were downloaded or received as shapefiles.

#### 4.1.2.2 Digital Elevation models

Two prepared digital elevation models (DEM) were included in the datasets used for this study. A 2020 LiDAR-based DEM of the study area was downloaded from Høydedata.no at no cost. Høydedata is an online platform that provides access to the elevation data resources of Kartverket. The DEM is a small part of the 1m resolution 2020 DEM of Jostedalsbreen developed from the LiDAR data by TerraTec as part of the National Detailed Height Model or nasjonal detaljert høydemodell (NDH) project.

Similarly, a 1966 DEM prepared at 8 m resolution from aerial photographs which was processed by Terretac for the entire Josteldalsbreen was made available by the Department of Geoscience, University of Bergen, Norway. The hill shades of both DEMs are shown in Figure 4.5.

#### 4.1.2.3 NVE glacier length data

The Norwegian Water Resources and Energy Directorate (NVE) publish the annual length observation of glaciers in Norway on its website (nve.no). The data is available for Briksdalsbreen from 1900 to 2015 and was freely downloaded for use in this study.

#### 4.1.2.4 Climate data

Plotted graphs and charts of summer temperature for Bergen and winter precipitation for western Norway based on data from eklima and Frost of the Nowagian Meteriological Institute was downloaded from Helge Drange page *( folk.uib.no/ngfhd/Climate/climate-pnor03.html).*

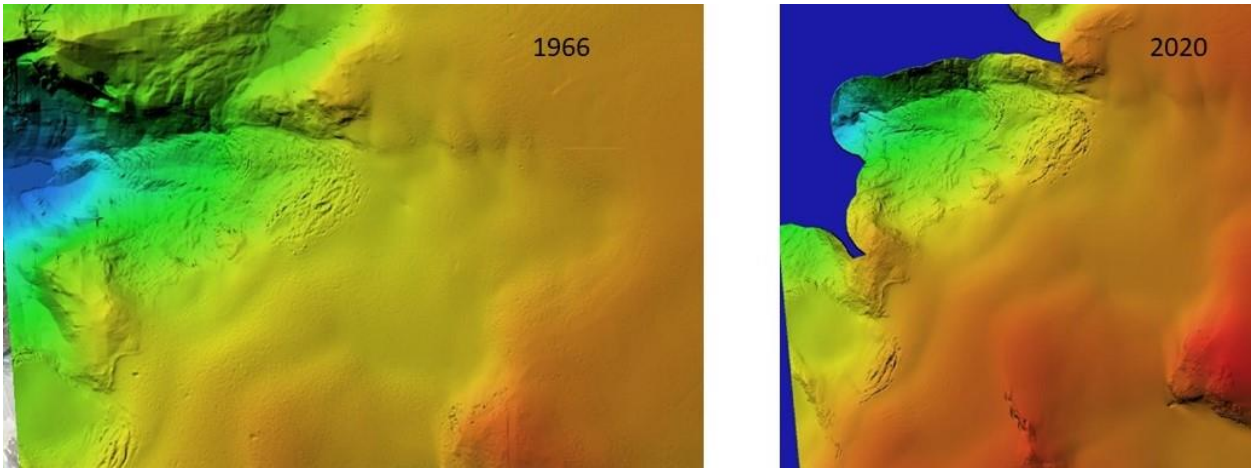


*Figure 4.5: Hill shades of 1966 and 2020 DEMs. 1996 DEM was provided by Department of Geoscience, University of Bergen and the 2020 DEM was downloaded from Høydedata.no*

## 4.2 Methods

Estimation of elevation changes and geodetic mass balance of glaciers is based on accurate digital elevation models (DEM). In this study, Agisoft Metashape professional software generated DEMs from scanned analogue and digital aerial photographs. Accuracy, precision estimation, and differencing of the generated DEM were performed with the XDEM python package. Glacier areas and length changes were estimated from the glacier outline in ArcGIS pro. Mass balance was computed from the elevation change and area information using a constant density of 850 ± 60 kg/m3. These procedures are summarized in Figure 4.6

### 4.2.1 DEM and Orthomosaic generation

All images were loaded into the Agisoft Metashape professional software and inspected for poor and unnecessary images. For all images in each set of aerial photographs, fiducial marks defining the camera coordinate system were collected and their coordinates were input. Likewise, other elements of interior orientation (calibrated focal length, principal point coordinates and radial distortion coefficient) were input as provided in the camera calibration report to ensure that accurate spatial information is determined from the images.

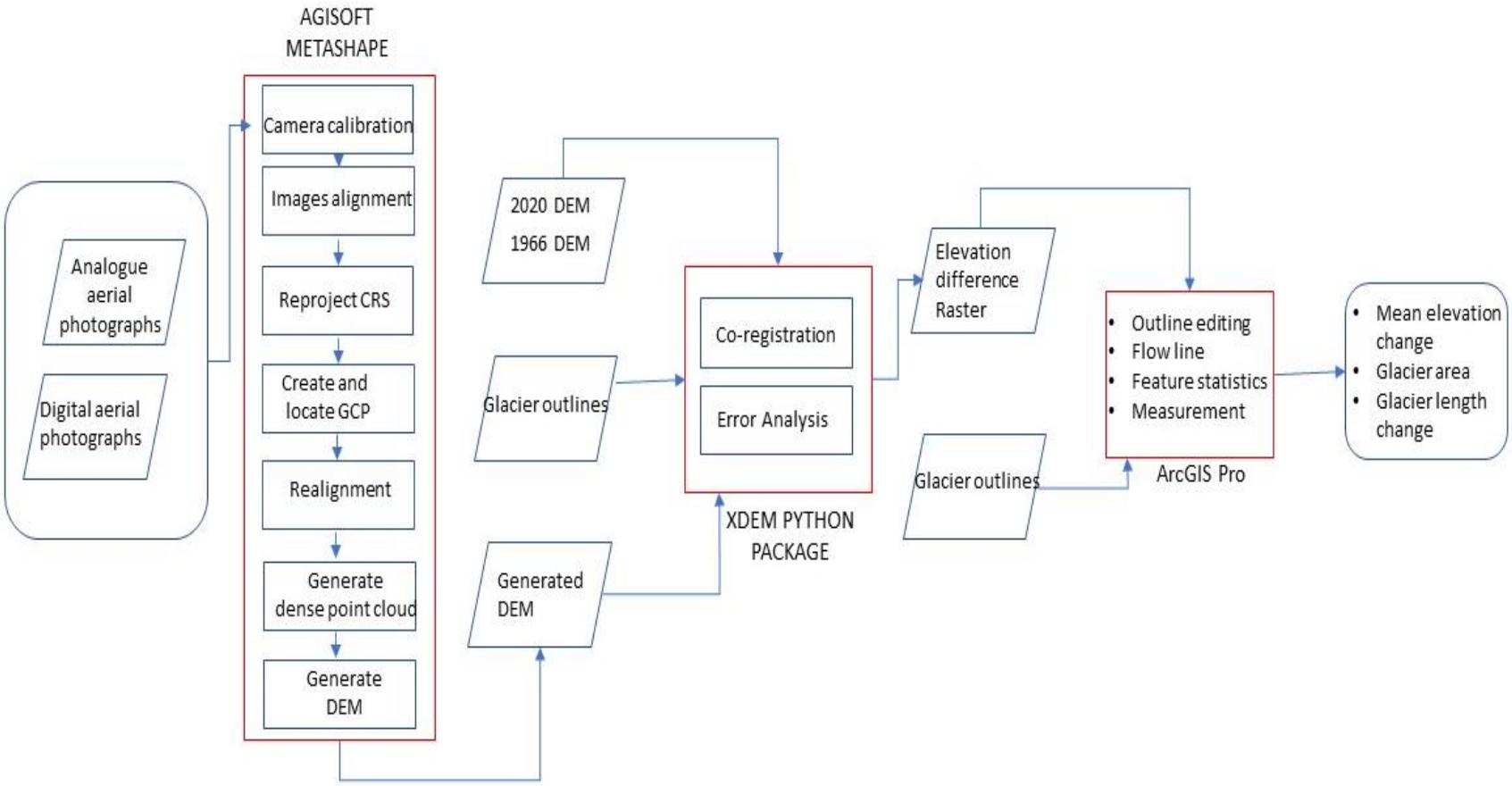


*Figure 4.6: Flow chart of image processing carried out in this study. Agisoft Metashape, ArcGIS pro and XDEM python package were used to extract glacier thickness, length change and area information from aerial photographs and DEMs.*

In the case of the 1960 dataset where the calibration parameters were not available, a self-calibration was performed by providing an estimated pixel size that was computed based on the resolution and format of the images. Areas outside the rectangular perimeters defined by the fiducial marks were masked to allow proper alignment of images and an automatic tie-point-based alignment was performed. In the next stage, ground control points (GCP) were collected by identifying selected features from the images on google earth and inputting the coordinates into the reference plane of the software. A minimum of three GCPs were used in each dataset and were sometimes extended with checkpoints collected by identifying the same features on at least three images. This process ensured the estimate of the position of the camera when the images were taken (exterior orientation), a condition necessary for DEM generation. The RMSE values for the collected GCPs are presented in Table 4.3 Beyond this stage, most of the processing was automated. Dense cloud and depth maps were built from which the DEMs were generated at 5 m resolution.

Unlike, analogue aerial photographs, processing of digital aerial photography is almost completely automated in Agisoft Metashape Professional. Insignificant camera distortion and the availability of precise pixel size and focal length allow an accurate estimation of the exterior orientation by the software. Only the focal length and pixel size were input, alignment, dense cloud building and DEM generation were performed automatically. The DEMs have a pixel size of 2 m and the orthomosaic images of each set of photographs were also produced from the dense cloud at the same resolution as their DEMs. Inspection and further analyses were conducted with ArcGIS pro.

#### 4.2.1.1 Co-registration and estimation of surface elevation change

The accuracy of a DEM is related to elevation biases caused by erroneous vertical shifts, tilts and horizontal referencing. If a stable terrain is present within the DEM, it is possible to align DEMs. This alignment of DEMs, termed co-registration provides a way to check the accuracy of a DEM when compared with accurate external reference DEMs or geolocated point elevation data and ensures correct estimation of elevation change DEMs. Co-registration of DEMs was performed with the XDEM python package based on the Nuth and Kääb (2011) approach. This approach models the probable offset direction by solving a cosine equation in a loop to determine the translation and bias correction.

*Table 4.3: RMSE of collected GCP for 1984, 1993 and 2001 dataset.*

| **1993** | | | | | |
|---|---|---|---|---|---|
| Label | X error(mm) | Y error(mm) | Z error(mm) | Total(mm) | Image (pix) |
| 1 | 0.06810 | -0.11016 | -0.12939 | 0.18307 | 0.425 |
| 2 | 0.04838 | 0.30962 | -0.07341 | 0.03218 | 0.792 |
| 3 | 0.10113 | 0.12413 | -0.06392 | 0.17240 | 0.685 |
| 4 | 0.07042 | 0.06650 | 0.08957 | 0.13193 | 0.647 |
| Total | 0.07444 | 0.17877 | 0.09252 | 0.21462 | 0.675 |
| | | | | | |
| **1984** | | | | | |
| Label | X error(mm) | Y error(mm) | Z error(mm) | Total(mm) | Image (pix) |
| 1 | -0.00241 | 0.00075 | -0.07612 | 0.07616 | 0.666 |
| 2 | 0.00040 | 0.00152 | 0.07264 | 0.07266 | 0.579 |
| 3 | 0.00122 | -0.00276 | 0.07638 | 0.07644 | 0.337 |
| 4 | 0.00084 | 0.00056 | -0.72919 | 0.07292 | 0.451 |
| Total | 0.00143 | 0.00164 | 0.07453 | 0.07545 | 0.501 |
| | | | | | |
| **2001** | | | | | |
| Label | X error(mm) | Y error(mm) | Z error(mm) | Total(mm) | Image (pix) |
| 1 | -0.31376 | 0.13163 | -0.20992 | 0.39980 | 0.729 |
| 2 | 0.11799 | -0.23549 | 0.14997 | 0.30310 | 0.484 |
| 3 | 0.19586 | 0.10403 | 0.05964 | 0.22966 | 0.511 |
| total | 0.22415 | 0.16694 | 0.15288 | 0.31856 | 0.601 |

Slope and aspect maps were generated from a glacier-masked reference (or Master) DEM and an elevation difference map was generated by comparing the reference DEM with the source (or slave) DEM. With these products, a cosine function is solved to obtain the most likely offset which is fixed by applying a suggested appropriate shift. The process is repeated iteratively until either spatial statistics normalised median absolute deviation (NMAD) stops improving significantly or the maximum iteration limit is reached. Shifts between the sets of DEMs differenced in this study are presented in Table 4.4.

Small rotations and non-linear biases were observed the DEMs generated from old aerial images. These were removed with the deramping script of XDEM which works by computing an N-degree polynomial over the entire difference between a reference and the DEM to be aligned. 1$^{st}$- degree deramping resulted in significant improvement in the elevation difference (Figure 4.7 and Table 4.5); the values NMAD and median over the stable ground reduced and the elevation difference is obtained with better accuracy. Applying a higher degree de-ramping created either no change or worsen the result. After successful co-registrations, outliers on the final elevation difference maps were filtered manually and the average change in elevation over the glacier was calculated and divided by the year interval between the two DEMs to obtain the change in elevation per year.

*Table 4.4: Linear shifts between pairs of co-registered DEM*

| Interval | X shift(Pixel) | Y shift(Pixel) | X shift(m) | Y shift(m) |
|---|---|---|---|---|
| 1966-1984 | 0.509 | 2.291 | 4.072 | 18.332 |
| 1984-1993 | -1.715 | -5.532 | -8.578 | -27.662 |
| 1993-2001 | 0.442 | -6.144 | 2.213 | -30.721 |
| 2001-2010 | -2.026 | -0.294 | -4.053 | -0.588 |
| 2010-2017 | -0.298 | -2.228 | -0.596 | -4.456 |
| 2017-2020 | 0.165 | 0.784 | 0.330 | 1.568 |
| 1966-2020 | 0.082 | 0.390 | 0.656 | 3.120 |

*Table 4.5: Values of NMAD and median over stable terrain before and after deramping. Deramping corrected the nonlinear bias and rotation between the pairs of DEMS. NMAD and median were greatly reduced.*

| Interval | Deramping Degree | NMAD before | NMAD after | Median before | Median after |
|---|---|---|---|---|---|
| 1993 - 2001 | 1 | 21.52 | 0.43 | -65.37 | 0.02 |
| 1984 - 1993 | 1 | 36.29 | 0.59 | -51.68 | 0.03 |
| 1966 - 1984 | 1 | 15.86 | 0.37 | 6.87 | -0.06 |

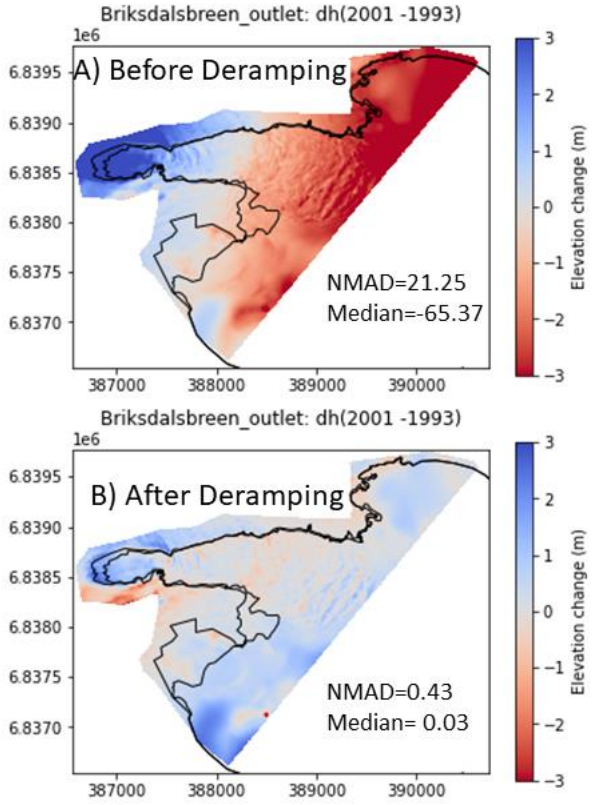


*Figure 4.7: Elevation difference map before and after decamping. Elevation difference map was improved significantly improved after deramping.*

#### 4.2.1.2 Elevation Change Uncertainty Assessment

The precision of a DEM depends on the Inherent variability of vertical precision (heteroscedasticity) and spatial correlation of errors. However, they can also be estimated by using a stable terrain as a proxy. Uncertainties in elevation changes were estimated based on the robust method presented by Huggonet *et al*, 2022 and implemented with the XDEM python package. If dh is the average of the elevation changes in area A, approximated by a disk of the same area, then for each pixel k in random subset of K pixel within the N pixels, the uncertainty in the spatial average $\sigma_{\overline{dh}}$ is given by,

$$\boldsymbol{\sigma^2_{\overline{dh}} \approx \overline{\sigma^2_{dh}|}\, A\, \frac{1}{N}\, \frac{1}{k} \sum_{k=1}^{K} \sum_{i=1}^{N} (1 - \gamma_{zdh}(x_k - x_i))} \qquad \textbf{(1)}$$

where $\overline{\sigma^2_{dh}|A}$ is the average variance of the elevation of pixel I in area A

$$\boldsymbol{\overline{\sigma^2_{dh}|A} = \frac{1}{N} \sum_i \sigma^2_{dh_i}} \qquad \textbf{(2)}$$

$\boldsymbol{\gamma_{zdh}(x_k - x_i)}$ is the spatial correlation between pixel k and i

#### 4.2.1.3 Estimation of glacier area and volume changes

The available polygons of the glacier outlines were edited in ArcGIS pro to fit the correct positions on each orthomosaic images and the areas representing each edited polygon were obtained from their attribute tables. An uncertainty 3% reported by Andreasson *et al.*, 2022 for the downloaded Norwegian glacier outlines was maintained in this study.

Changes in volume was estimated by multiplying the average elevation changes of the glacier by the glacier area (equation 3) and the uncertainty $\sigma_{\Delta V}$ in volume was computed with the following equation 4.

$$\boldsymbol{\Delta V = dh \times A} \qquad \textbf{(3)}$$

$$\boldsymbol{\sigma_{\Delta V} = \Delta V \sqrt{\frac{\sigma^2_{\Delta v}}{\Delta V^2} + \frac{\sigma^2_A}{A^2}}} \qquad \textbf{(4)}$$

where $\sigma_A$ is the uncertainty in area A

#### 4.2.1.4 Estimation of mass balance

The geodetic mass balance was calculated with the following equation.

$$B_{geod} = \frac{\Delta V \times f_{\Delta v}}{A_N} \qquad (5)$$

$f_{\Delta v}$ is the conversion factor = 850 ± 60 (Huss, 2013) for density (ρ) glacier ice taken as on 850 ± 60 Kgm$^{-3}$. $A_N$ is the area of the first year used to normalize the mass balance values so that they can be compared easily.

If $\sigma_\rho$ is the uncertainty in density ( ± 60 Kgm$^{-3)}$ ), then The uncertainty in mass balance, $\sigma_B^2$ is given by:

$$\frac{\sigma_B}{B_{geod}} = \sqrt{\frac{\sigma_{\Delta V}^2}{\Delta V^2} + \frac{\sigma_\rho^2}{\rho^2} + \frac{\sigma_A^2}{A^2}} \qquad (6)$$

#### 4.2.1.5 Estimation of changes in glacier length

Glacier length is estimated by measuring the distance between glaciers outlines along a manually digitized central flowline (Figure 4.8) that is based contour map generated from the 2020 DEM. Since the glacier outline used in the study are majorly digitized from a 30m resolution LandsatTM scenes, the uncertainty in the measured length cannot be less than 30 meters.

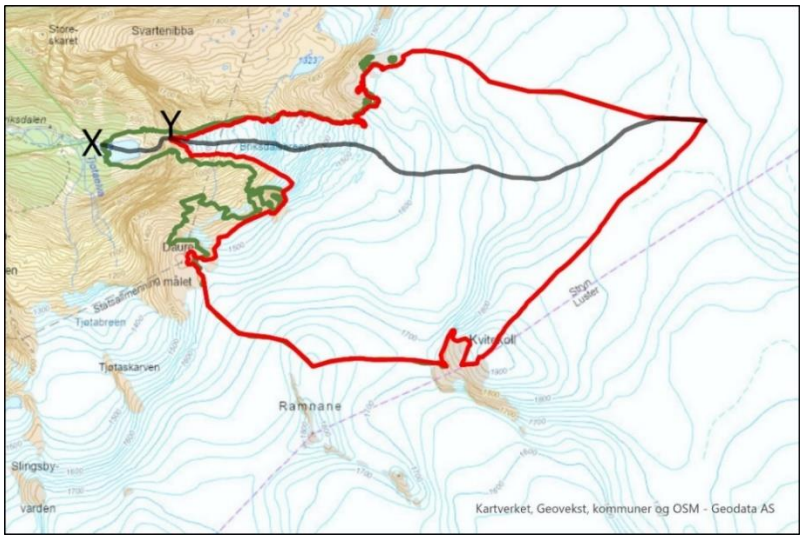


*Figure 4.8 Lengths are measured along the central flow lines (BLACK) between point X and Y where it intersects the glacier outline (Red and Green)*

# Chapter 5 : Results

The results of this study are presented in this chapter.

## 5.1 Surface elevation change

Table 5.1 and Figure 1 present the summary of the surface elevation changes obtained in this study. The results show a thickening of the glacier front between 1966 to 2001 and a thinning of the front and total glacier between 2001 – 2010 and 2010 – 2020 respectively (Figure 5.2 – 5.5). The surface of Briksdalsbreen lowered by a mean of - 0.06 ± 0.01 m $a^{-1}$ between 1966 – 2020 with an average of -2.98 ± 0.60 m in the entire 54 years period. Nevertheless, the greatest surface lowering (> 50 m) occurred towards the glacier terminus between 500 m and 1000 m a.s.l (Figure 5.2) whereas the uppermost boundary of the glacier catchment showed only a slight surface reduction (< - 0.5 m). Between 2017 – 2020, the glacier thinned by an average of -0.82 ± 0.45 m in total, indicating an annual loss of surface ice with average thickness of 0.27 ± 0.15m. The highest ablation rate in this period also at the glacier terminus where its surface elevation lowered by more than 20 m. Compared with 2017 – 2020, the glacier surface thinned a little faster (-0.30 ± 0.2 m $a^{-1}$) in 2010 – 2017; within this 7 years period the surface of Briksdalsbreen lowered by an average of - 2.08 ± 1.03 m with greater values (> 34 m) also recorded in the glacier toe. In total Briksdalsbreen lowered by an average of – 2.87 ± 0.94 m between 2010 and 2020.

Only the thickness of the glacier front was measured for 1966 – 1984, 1984 – 1993, 1993 – 2001 and 2001- 2010 based on the available datasets. However, estimation of the glacier front was based on a comparable extent of the glacier. The results reveal that the surface elevation increased by 0.01 ± 0.01 m $a^{-1}$ for a period of 1966 – 1984, but at a much faster rate (0.04 ± 0.01 m $a^{-1}$) between 1984 – 1993. This rate was maintained in 1993 – 1984 but reduced between 2001 – 2010 when the glacier front thinned by -0.06 ± 0.01 m $a^{-1}$. Changes in surface elevation of the glacier are generally small and may be related to high steepness of the front of the glacier that enables a rapid movement of ice masses down slope to ablation areas where they melt easily in warm summers.

*Figure 5.1: Mean surface elevation change of Briksdalsbreen between 1966 - 2020. Red represents thinning while the blue shows thickening.*

| Year Interval | Coverage | Total mean surface change (m) | Annual mean surface change ($ma^{-1}$) |
|---|---|---|---|
| 1966 - 1984 | Glacier front | 0.24 ± 0.04 | 0.01 ± 0.00 |
| 1984 - 1993 | Glacier front | 0.39 ± 0.05 | 0.04 ± 0.01 |
| 1993 - 2001 | Glacier front | 0.30 ± 0.08 | 0.04 ± 0.01 |
| 2001 - 2010 | Glacier front | -0.53 ± 0.05 | -0.06 ± 0.01 |
| 2010 - 2017 | Whole Glacier | -2.08 ± 1.30 | -0.30 ± 0.20 |
| 2017 - 2020 | Whole Glacier | -0.82 ± 0.45 | -0.27 ± 0.15 |
| 2010 - 2020 | Whole Glacier | -2.87 ± 0.94 | -0.29 ± 0.10 |
| 1966 - 2020 | Whole Glacier | -2.98 ± 0.60 | -0.06 ± 0.01 |

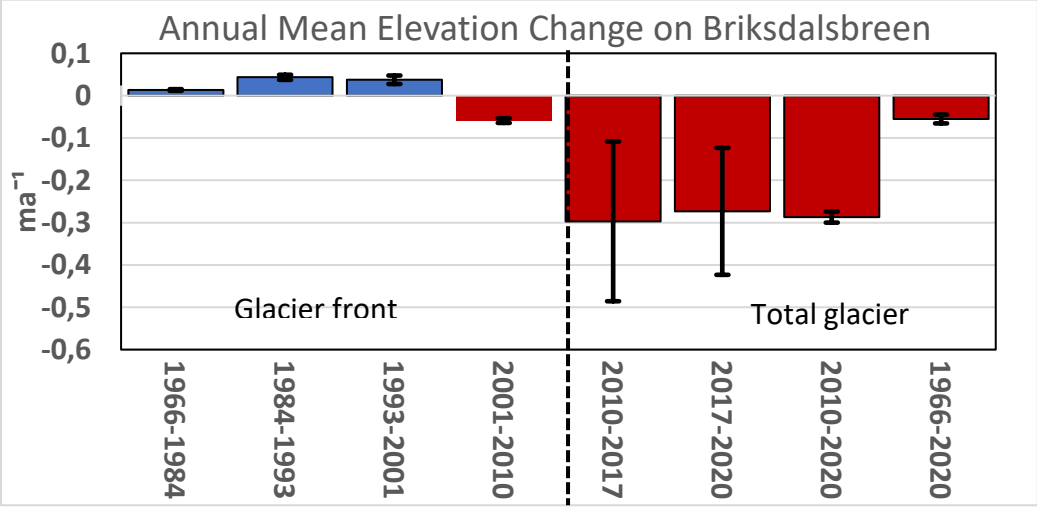


*Table 5.1: Summary of mean surface elevation change of Briksdalsbreen between 1966 - 2020.*

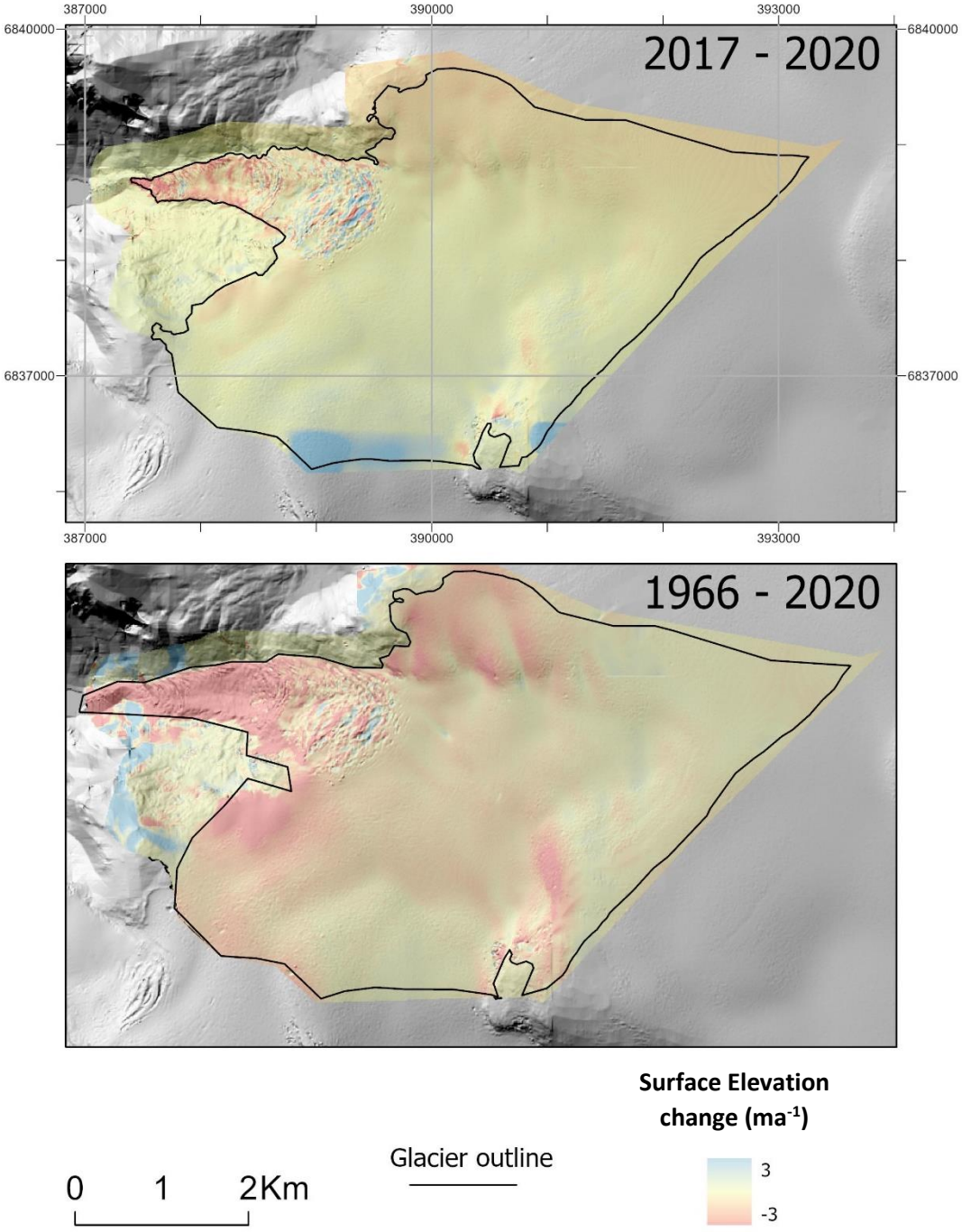


*Figure 5.2: Mean annual surface elevation change of entire Briksdalsbreen between 2017 – 2020 and 1966 – 2020.*

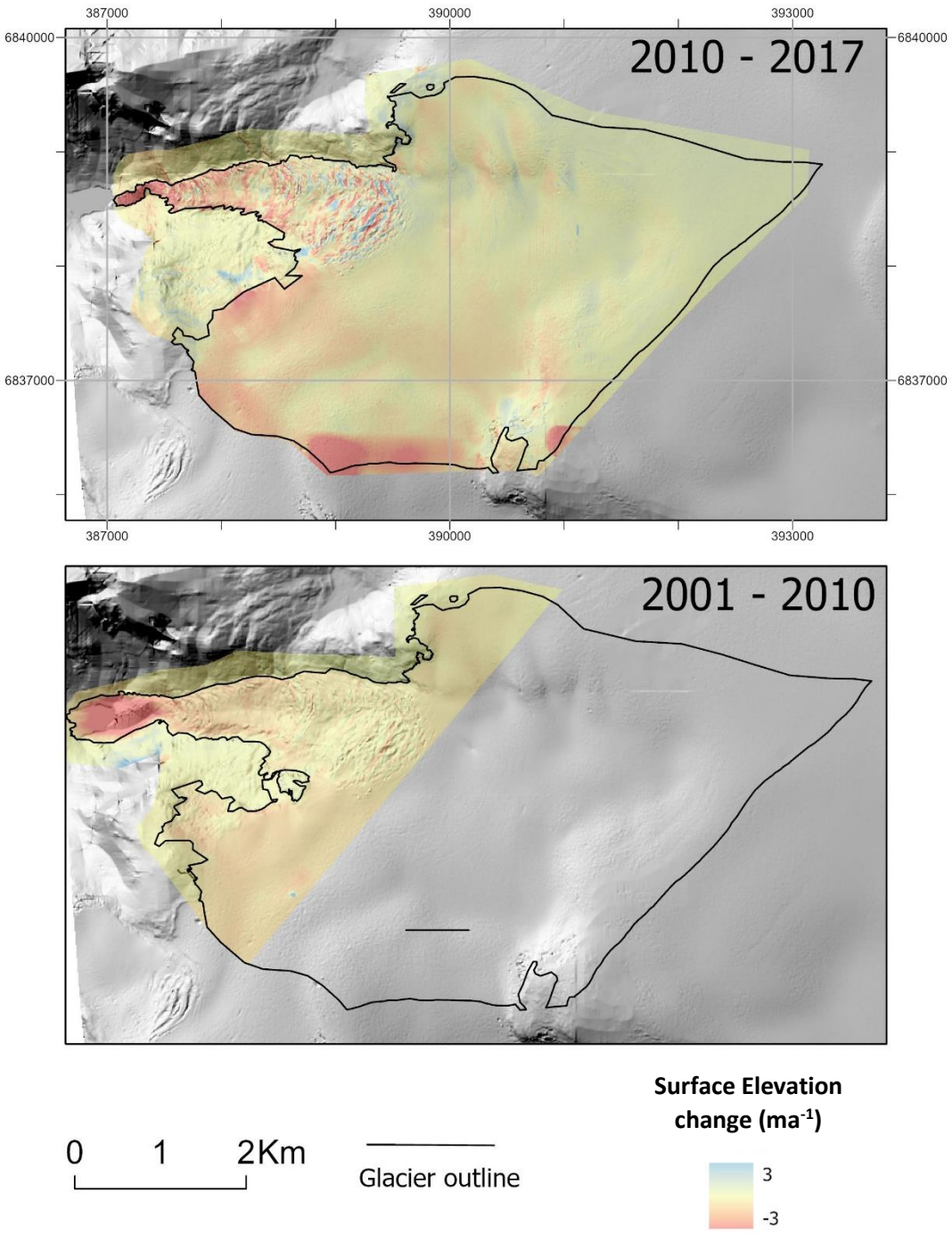


*Figure 5.3: Mean annual surface elevation changes of the entire of Briksdalsbreen between 2010 – 2017 and the glacier front between 2001 – 2017.*

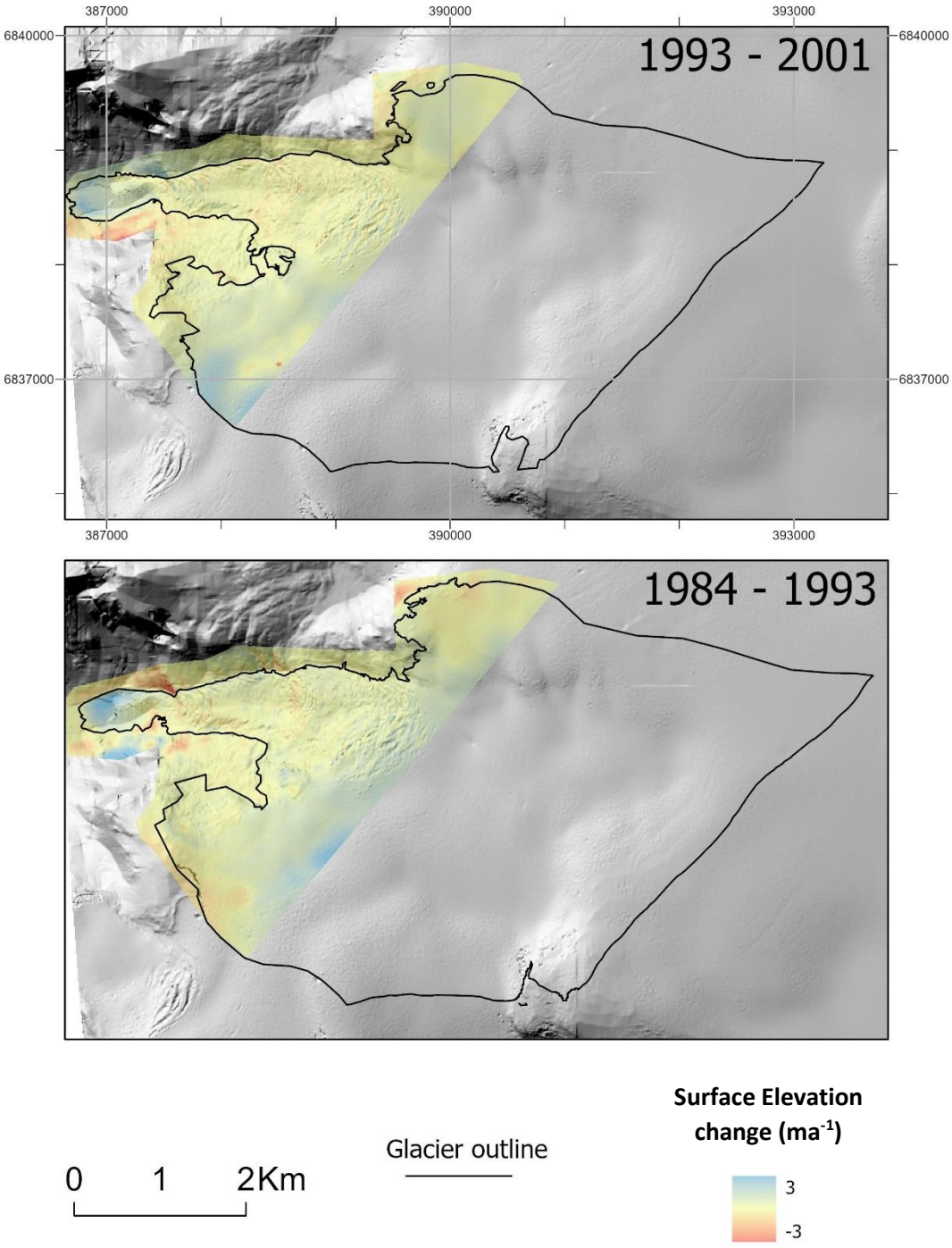


*Figure 5.4: Mean annual surface elevation changes frontal part of Briksdalsbreen between 1993 – 2001 and 1984 – 1993.*

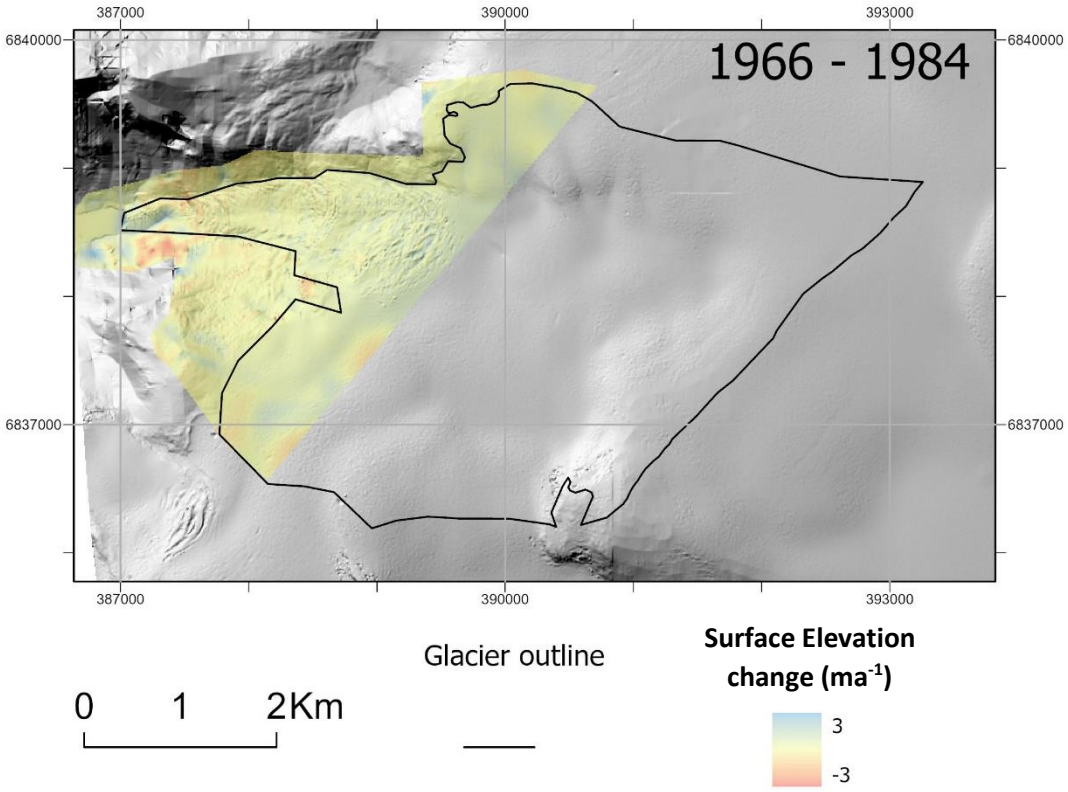


*Figure 5.5: Mean annual surface elevation changes frontal part of Briksdalsbreen between 1984 – 1966*

The Change in mean surface elevation per year per altitude band for different investigated time periods are shown in Figure 5.6 and 5.7. They show a decreasing rate of thinning towards the higher part of the glacier. Although the average change in surface elevation of the glacier front for the periods investigated between 1966 – 2001 are positive, some sections between 550 m and 850 m are lowered during the period of 1966 – 1984 and 1984 – 1993. The elevation profile also shows a higher rate of thinning in 2017 – 2020 than 2010 – 2017 indicating an increasing thinning rate in more recent time.

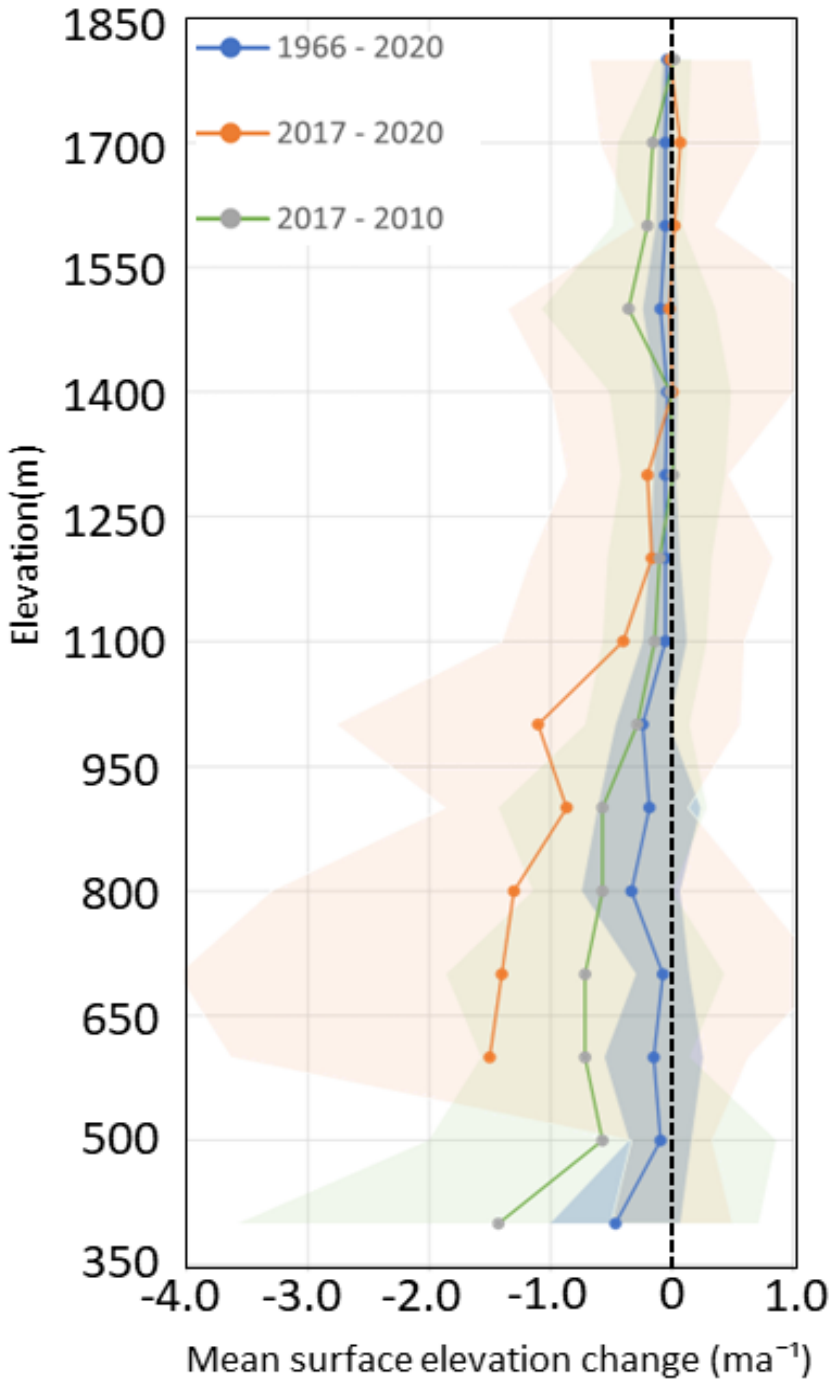


*Figure 5.6 Change in mean surface elevation per year per altitudinal band for the different 2010- 2017, 2017-2020 and 1966-20202 for Briksdalsbreen Glacier. Shaded error bars represent the standard deviation at each elevation band.*

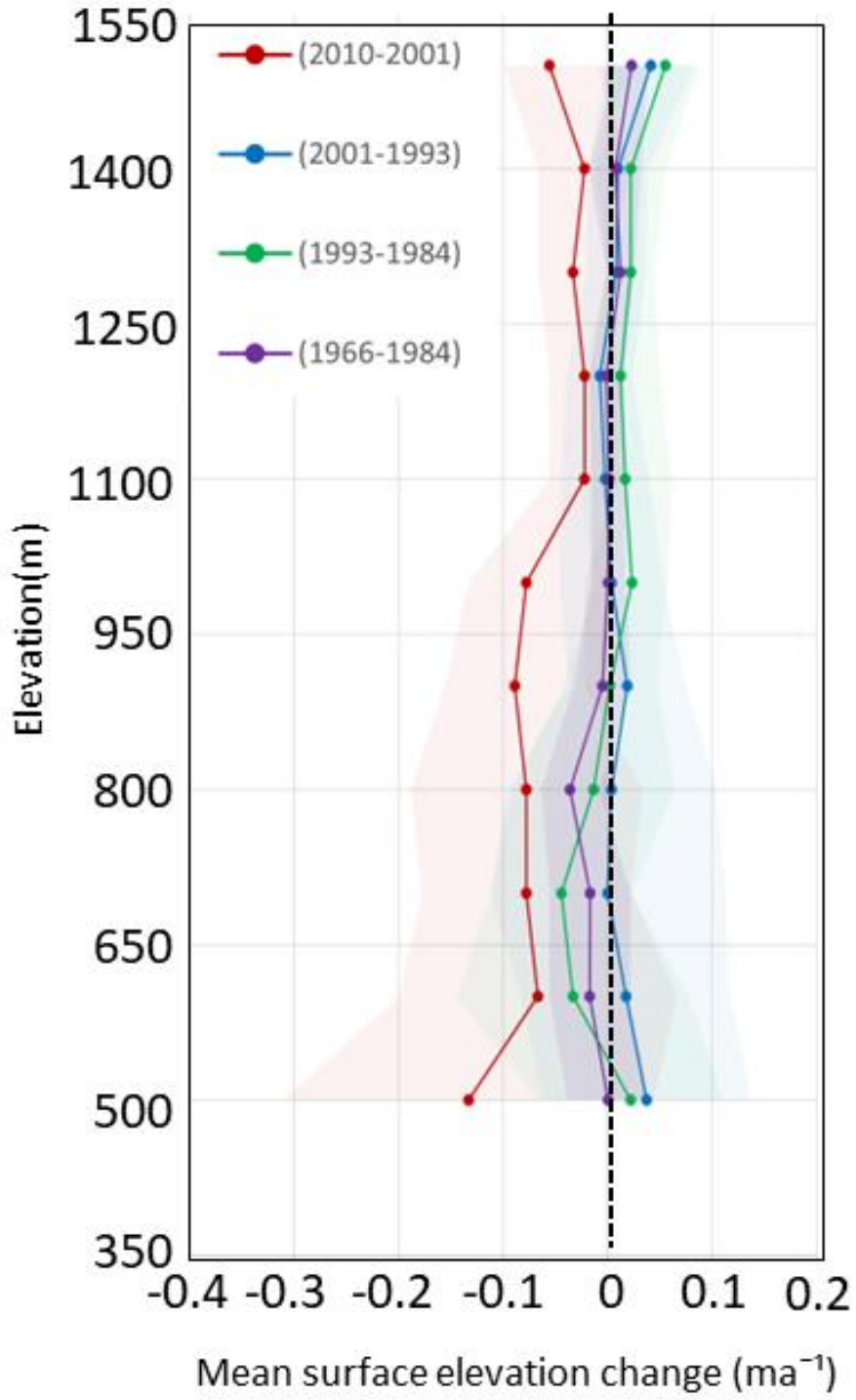


*Figure 5.7: Change in mean surface elevation per year per altitudinal band in the period of1966 – 1984, 1984 – 1993, 1993 – 2001 and 2001- 2010 for the frontal part Briksdalsbreen Glacier. Shaded error bar represents the standard deviation at each elevation band.*

## 5.2 Area Change

The total estimated area of Briksdalsbreen in 1966 is 11.77 ± 0.35 $Km^2$ (Table 5.2). Fifty-four (54) years after, (1966 – 2020), the glacier has shrunk by a total of 0.25 ± 0.05 $Km^2$ (- 2.17 ± 3.00 %) at a mean rate of -0.04 ± 0.01% $a^{-1}$ although it only began a persistent shrinkage after a period of expansion. The glacier expanded between 1966 to 1984 by almost the same amount of area it shrunk in 1966 - 2020 thereby spreading at an average of 0.11± 0.02 % $a^{-1}$ and eventually occupied an additional 7.6 ± 0.02 % of its 1966 total area in 2001. In this year (2001), the total estimated area of Briksdalsbreen had increased to 12.67 ± 0.35 $Km^2$. Since 2001, Briksdalsbreen has shrunk at an average rate of – 0.44 ± 0.14 % $a^{-1}$ until 2020, however, it had the highest average annual rate of diminishing area between 2017 – 2020.

In this study, the frontal part of the Briksdalsbreen is taken as the section of the glacier below an elevation of 1550 m where there is sharp change in elevation gradient. Changes in the extent (Figure 5.8 and 5.9) of this front is significant and the part above it has maintained a constant area over the years. The area of the glacier front in 1966 was 1.64 ± 0.05 $Km^2$ and it increased to 2.54 ± 0.08 $Km^2$. Between 2001 and 2010, the glacier front shrunk by ∼49%. In 2020 the area of the glacier fronts is only ∼80% of its 1966 area.

## 5.3 Length Change

As shown in Table 5.3 and Figure 5.10, the terminus of Briksdalsbreen retreated by - 456 m in total at a rate of - 8.4 m $a^{-1}$ between 1966 to 2020. In 1966, the frontal part of Briksdalsbreen terminated in lake Briksdalsvatn (Figure 5.9) and covered less than a quarter of the lake; however, in 2001, more than three- quarter of the lake was covered by the glacier. In this period (1966 – 2001), Briksdalsbreen increased in length by 321 m and advanced at an average rate of 6.1 m $a^{-1}$, 12.7 m $a^{-1}$and 12.3 m $a^{-1}$ for the periods 1984-1966, 1984-1993 and 1993-2001 respectively. In 2010, the glacier terminus had withdrawn slightly out of Lake Briksdalsvatn after it had retreated a total of -448 m at an average of -49.7 m $a^{-1}$. Likewise, the glacier front retreated -395 m in total in 2017 at -56.0 m $a^{-1}$ to a higher elevation than 2010. Briksdalsbreen retreated an additional -10 m between 2017 and 2020 and its terminus was pushed further higher (Figure 5.11).

*Table 5.2: Area of Briksdalsbreen between 1966 - 2020*

| Year | Area ($Km^2$) | Area change ($Km^2$) | Area change ($\% a^{-1}$) |
|---|---|---|---|
| 1966 | 11.77 ± 0.35 | - | - |
| 1984 | 12.02 ± 0.36 | 0.25 ± 0.50 | 0.11 ± 0.02 |
| 1993 | 12.53 ± 0.38 | 0.51 ± 0.50 | 0.45 ± 0.04 |
| 2001 | 12.67 ± 0.38 | 0.14 ± 0.60 | 0.14 ± 0.05 |
| 2010 | 12.63 ± 0.35 | -0.04 ± 0.50 | -0.04 ± 0.01 |
| 2017 | 11.58 ± 0.35 | -0.05 ± 0.50 | -0.06 ± 0.05 |
| 2020 | 11.52 ± 0.35 | -0.06 ± 0.50 | -0.17 ± 0.11 |
| Total | | -0.25 ± 0.05 | -0.04 ± 0.01 |

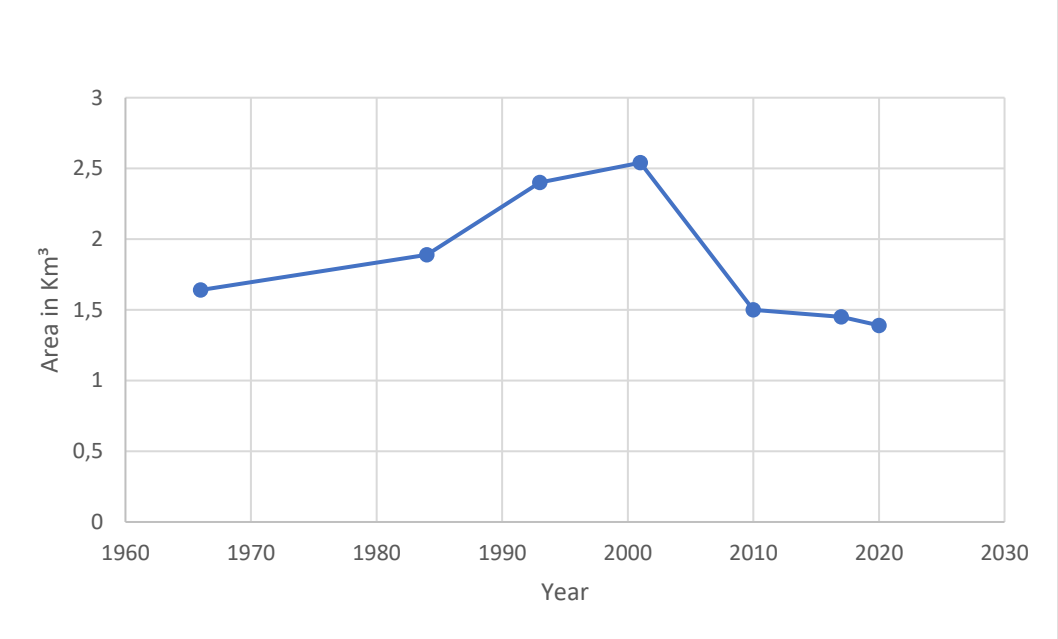


*Figure 5.8: Trend of total area changes in front Briksdalsbreen between 1966 – 2020. The total area increased in the 1990s and decreased by 2020s. Error in the area is taken as 3%.*

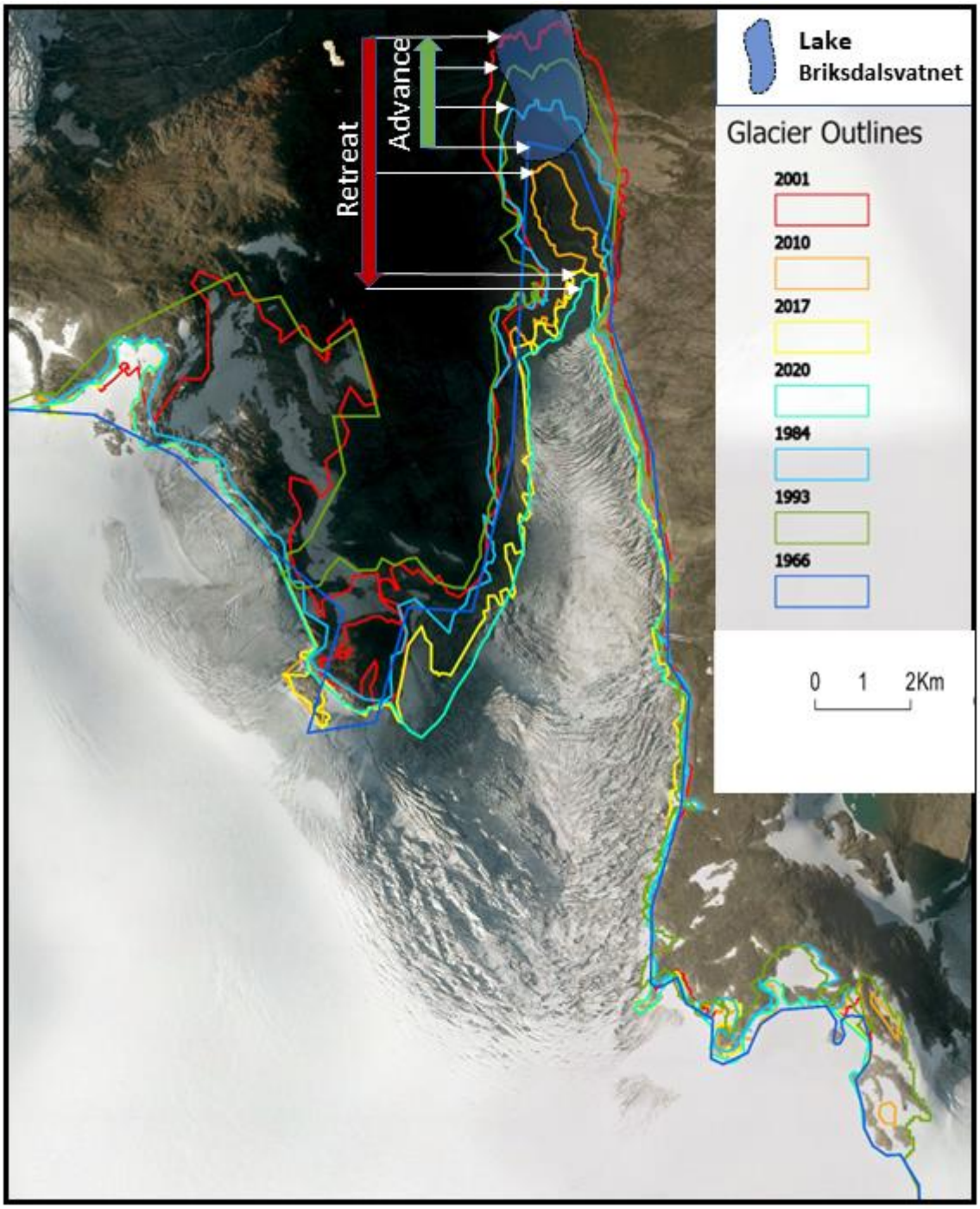


*Figure 5.9: Outlines of the extent of Briksdalsbreen between 1996 - 2020 on the 2017 orthomosaic image. The glacier expanded over lake Briksdalsvatnet from 1966 to 2001 and have shrunk back far away from the lake by 2020.*

*Table 5.3: Total length change and change in length per year in Briksdalsbreen from 1966 - 2020*

| Interval | Total Change in length (m) | Change in length/year ($ma^{-1}$) |
|---|---|---|
| 1966-1984 | 144 | 6.1 |
| 1984-1993 | 114 | 12.7 |
| 1993-2001 | 98 | 12.3 |
| 2001-2010 | -448 | -49.7 |
| 2010-2017 | -395 | -56.0 |
| 2017-2020 | -10 | -3.3 |
| 1966-2020 | -454 | -8.4 |

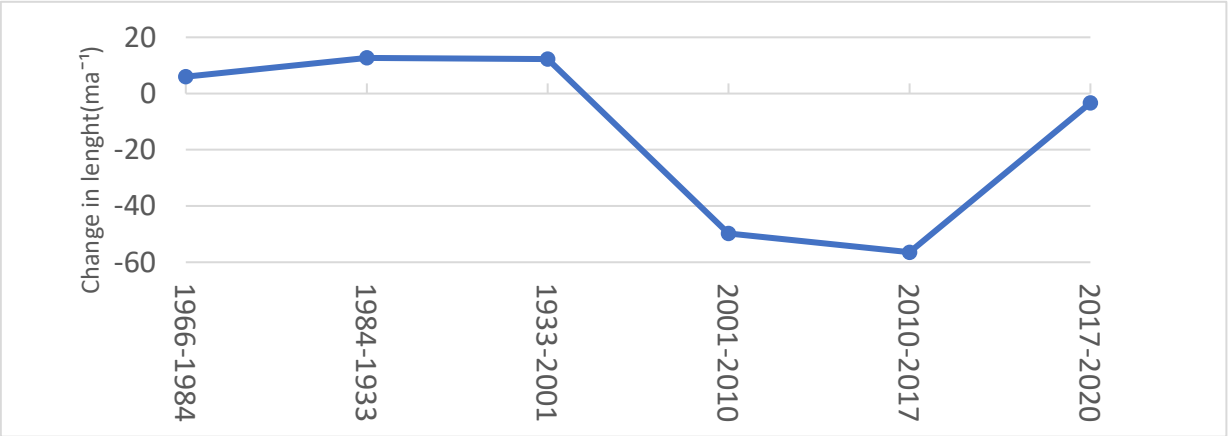


*Figure 5.10: Length changes per year in Briksdalsbreen between 1966 – 2020.*

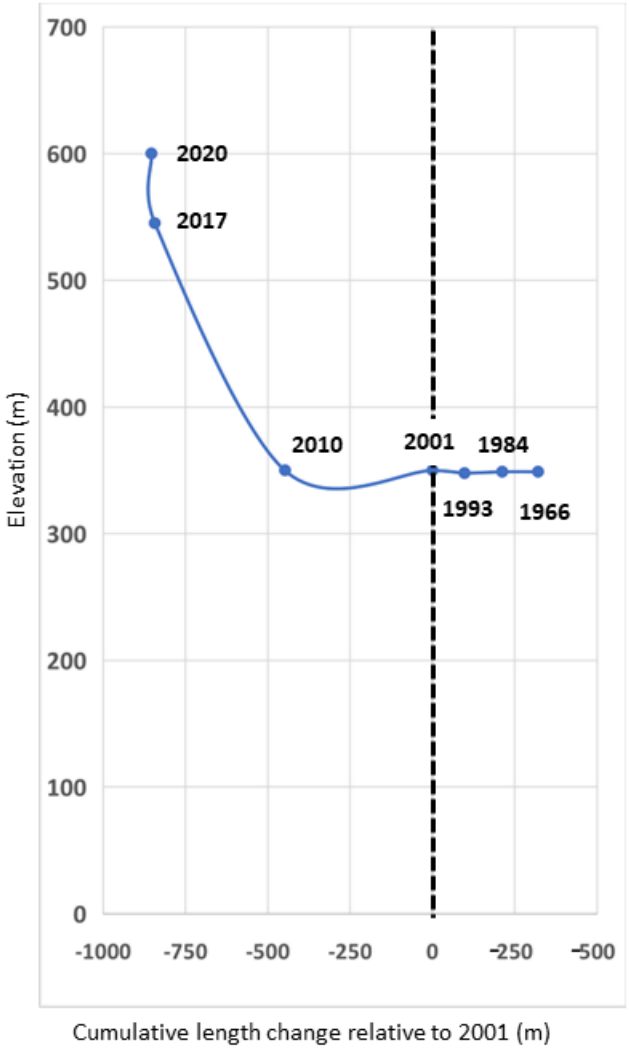


*Figure 5.11: Relative cumulative change in length across the elevation of Briksdalsbreen. Length changes are measured relative to 2001.*

As shown in Figure 5.11, the advance of the front of Briksdalsbreen in the 1990s and its retreat in first decade of the 21st century took place at an approximate flat surface of ~350 m a.s.l. Between 2010 and 2017 the glacier retreated to an elevation of 545 m along its steep valley and by 2020, the front of  stood at ~600 m a.s.l,

## 5.4 : Volume Change and Mass balance

Briksdalsbreen lost a total 2884866 ± 429519 $m^3$ of ice between 1996 – 2020 and a mean of -160270 ± 23862 $m^3$ $a^{-1}$. It accumulated the greatest amount of ice between 1984 – 1993 at an average rate of 543350 ± 76978 $m^3$ $a^{-1}$ and lost the greatest volume (-33378189 ± 7510273 $m^3$ in total) of ice in the period 2001 – 2007 at a mean rate of -33378189 ± 751027 $m^3$ $a^{-1}$.

The result shows a mass balance of -0.045 ± 0.05 m w. e. $a^{-1}$ for Briksdalsbreen in the period of 1966-2010. The mass balance of the glacier reduced slightly from -0.25 ± 0.01 to -0.23 ± 0.20 m w. e. $a^{-1}$ for time intervals 2010 - 2017 and 2017 - 2020. Considering the whole 10 years between 2010 – 2020, the mass balance of the glacier is -0.25 ± 0.01 m w. e. $a^{-1}$.

*Table 5.4: Table 5.4 Total Volume change, Volume change per year, and mass balance of Briksdalsbreen between 1966 – 2020.*

| Interval | Coverage | Total Volume change ($m^3$) | Volume change ($m^3$ $a^{-1}$) | Mass balance (m w. e. $a^{-1}$) |
|---|---|---|---|---|
| 1966 - 1984 | Glacier front | 2884865,5 ± 429519 | 160270,3 ± 23862 | - |
| 1984 - 1993 | Glacier front | 4890150,8 ± 692808 | 543350,1 ± 76978 | - |
| 1993 - 2001 | Glacier front | 3801665,4 ± 1020172 | 475208,2 ± 127521 | - |
| 2001 - 2010 | Glacier front | -6716276 ± 664876 | -746253 ± 73875 | - |
| 2010 - 2017 | Total Glacier | -24190465 ± 15368784 | -3455781 ± 2195541 | -0.254 ± 0.010 |
| 2017 - 2020 | Total Glacier | -9494120 ± 5217976 | -3164707 ± 1739322 | -0.233 ± 0.200 |
| 1966 - 2020 | Total Glacier | -35087711 ± 10396891 | -649772 ± 377720 | -0.045 ± 0.050 |
| 2010 - 2020 | Total Glacier | -33378189 ± 7510273 | -3337819 ± 751027 | -0.246 ± 0.010 |

# Chapter 6 : Discussion

In this section, results from this study are compared with field data, regional glacier change studies as well as changes of other Norwegian glaciers. How climate relate with the estimated changes is discussed and potential sources of uncertainty were also examined.

## 6.1 Comparison with field measurement

Only the annual field observations of length change are available for Briksdalsbreen. The trend of the annual length change observation of Briksdalsbreen by the NVE agrees with the outcome of this study (Figure 6.1), however, this study underestimated the mean length change per year by 1.0 – 2.0 m $a^{-1}$. Field data were acquired annually; therefore, they show detailed variable annual change in length of Briksdalsbreen, but this variability was not captured in this study since the estimated change per year are based on the total change between two time periods (Figure 6.2). For example, the retreat of 1970, 1971, 1972 and 1973 (11 m, 7 m, 7 m and 20 m respectively) were interpreted as an advance of 9 m $a^{-1}$ in this study. Likewise, Briksdalsbreen advanced more than 9 m $a^{-1}$ in 1975, 1976, 1977, 1979 and 1980. Between 1984 and 1993, field data showed a steady retreat of 7 m in 1985, 1986 and 1987 while this study obtained an estimated average advance of 12.7 m $a^{-1}$ for these years. Based on field measurement, the beginning of the current incessant recession of the glacier was 1997 after the glacier advanced 80 m $a^{-1}$ between 1994 and 1997. However, the coarse temporal resolution of the selected time interval (1993 - 2001) could not resolve this detail consequently in this study, hence, |the retreat of Briksdalsbreen was generalised to commence in 2001. Similarly, the less negative changes in length of Briksdalsbreen in 2012 was not captured although a significant less mean annual retreat between 2010-2017 and 2017-2020 was identified. Nevertheless, the total length changes between the investigated periods are quite similar for both field observation and estimate from remote sensing. If annual remotely sense data were available, it may be possible replicate the field data with a higher accuracy.

To the knowledge of the author at the time of this study, there are no official publication of field observation of mass balance in Briksdalsbreen. Therefore, comparison of glaciological mass balance from field measurement with the geodetic mass balance from of this study cannot be achieved. However, the annual observations from several other glaciers in Norway are available and section 6.4 discusses how the result from study compares with other glacier observations in Norway.

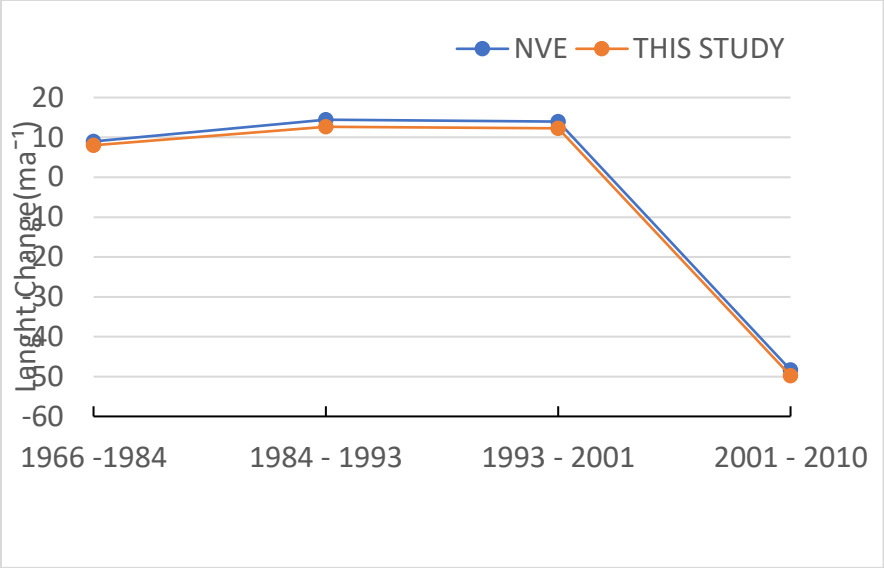


*Figure 6.1: Comparison of average annual length changes in this study with the average annual observed changes reported by the NVE on Briksdalsbreen between 1966 - 2010. NVE data is only available up to 2015. The changes in length have similar trend and close values with a difference of 1 – 2 m $a^{-1}$*

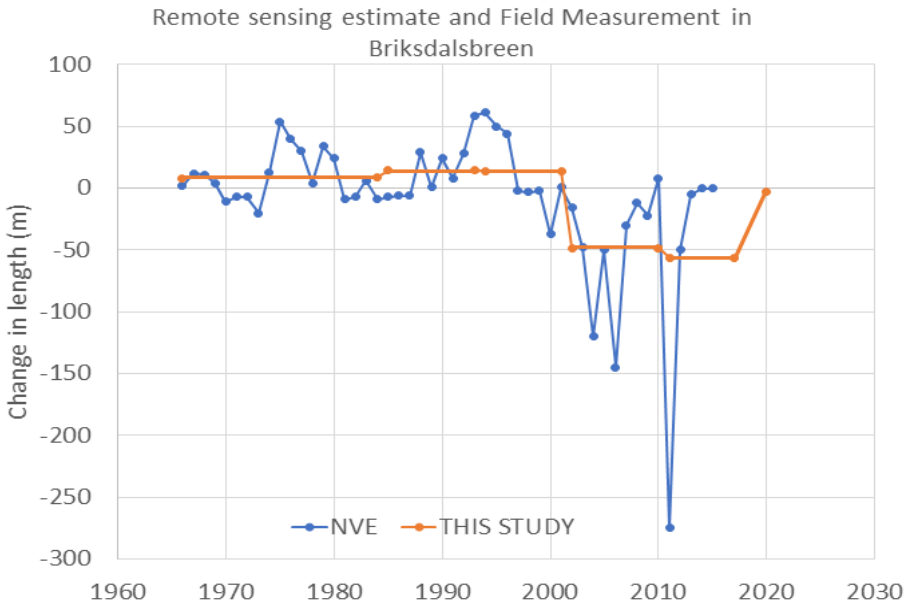


*Figure 6.2: Comparison of the mean annual change in length from this study with the true annual change in length from NVE measurement. The Estimated length change in this study did not capture the variability between intervals of each set of years measured.*

### 6.2 Comparison with regional remote sensing studies covering Briksdalsbreen.

A recent study by Hugonnet et al, 2021 utilized mulit-temporal ASTER DEM at 30 m resolution to compute global ice loss between 2000 - 2020. The mean surface elevation changes per year (-0.3 m $a^{-1}$) obtained for Briksdalsbreen in the study between 2010 – 2020 is comparable to the 0.29 ± 0.1 m $a^{-1}$ for the same period despite the difference in spatial resolution. The elevation profiles (Figure 6.3 and 6.4) from both studies also agree well at elevation above 900 m. Values from Hugonnet et al, 2021 are 1 – 3 m $a^{-1}$ more positive below 900m. Disparity between the result below 900 m may be linked to the coarse spatial sampling of Hugonnet et al, 2021. Also, the aerial photo used in this study was acquired in summer (July) while the 2010 dataset used by Hugonnet et al, 2021 was dated 1$^{st}$ of Jananury summer. The glacier front must have melted before the 2010 dataset used in this study was acquired. Nevertheless, both a showed lesser thinning towards higher elevation (Figure 6.4) although the result from Hugonnet et al, 2021 show a larger spread and error. Periods between 2001 – 2020 for this study and 2001 – 2010 for Hugonnet et al, 2021 were also compared. The results agreed quite well and as expected the result from Hugonnet et al, 2021 was more negative especially in the glacier front (400 – 900m) because it included an extra year of ablation. Although, regional studies covering Briksdalsbreen using remote sensing are few to allow more assessment, comparison with Hugonnet et al, 2021 showed that the result from this study conform with regional studies and identified the capability of remote sensing in providing useful consistent results.

The glacier outlines used in this study were made from regional mapping of glaciers for periods between 1988 – 1997 and 1996 – 2006 using Landsat scenes and 2017 – 2018 using Sentinel images. They had to be manually edited to fit the years investigated in this study. The obtained areas (12.02 ± 0.36 $Km^2$) is comparable with the published area of Briksdalsbreen by the NVE (11.94 $Km^2$)

### 6.3 Comparison with measurement from other glaciers in Norway

Surface change estimation of the neighbouring glaciers of Briksdalbreen (Nigardsbreen, Bergsetsbreen and Baklibreen) between 1984 -1993 and 1993 – 2001 was made by Wangensteen et al., 2006 using aerial photographs. They found that the frontal part Nigardsbreen thinned by an average of -3.3 ± 7.1 m between 1984 – 1993 although its lower part (675 m) thickened by 5 - 6 m. In 1993 – 2001. During the same period an average 0.39 ± 0.05 m thickening was estimated for

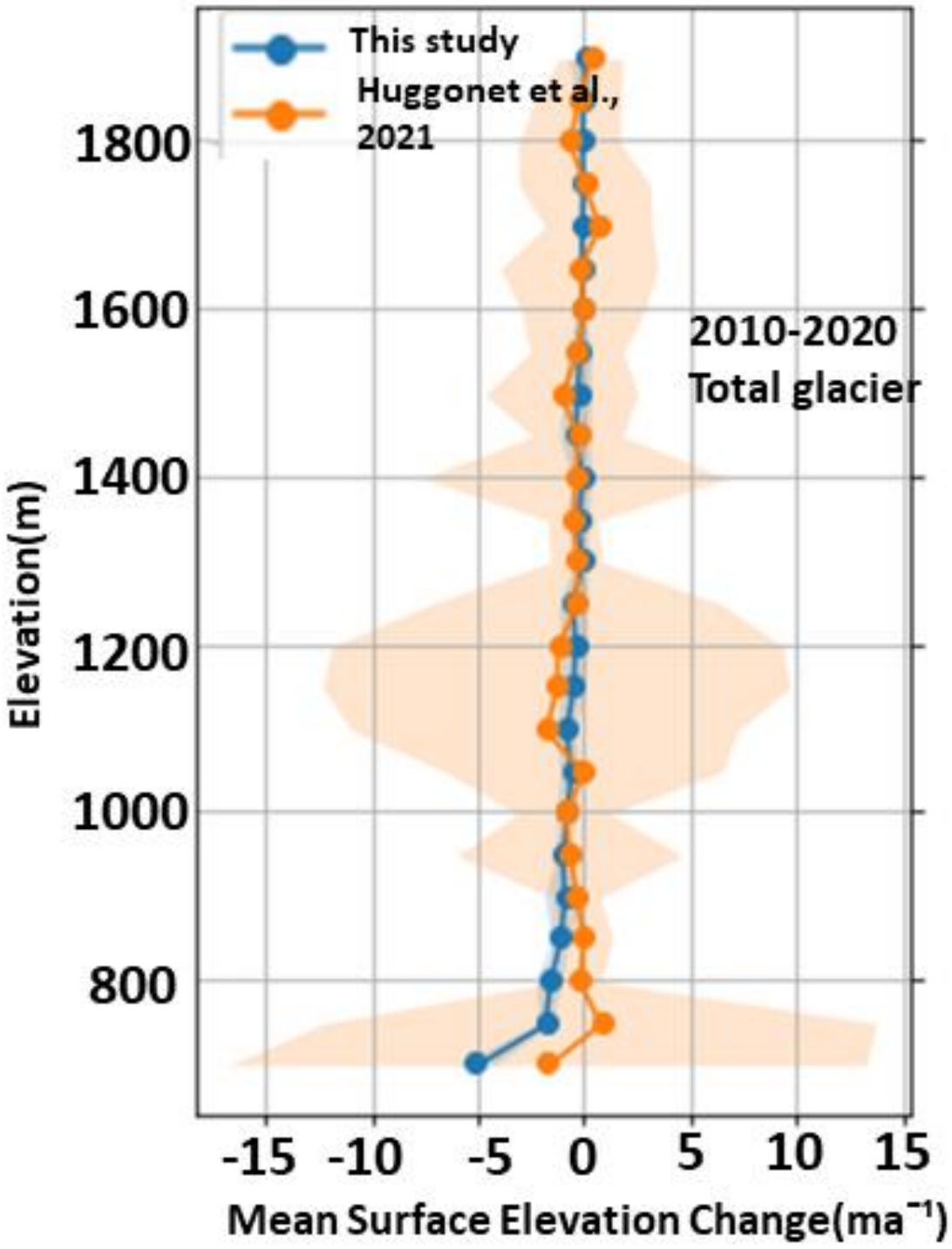


*Figure 6.3: Change in mean surface elevation per year per altitudinal band for the different 2010- 2020 for this study and Hugonnet et al.,2021. Shaded error bars represent the error for each study.*

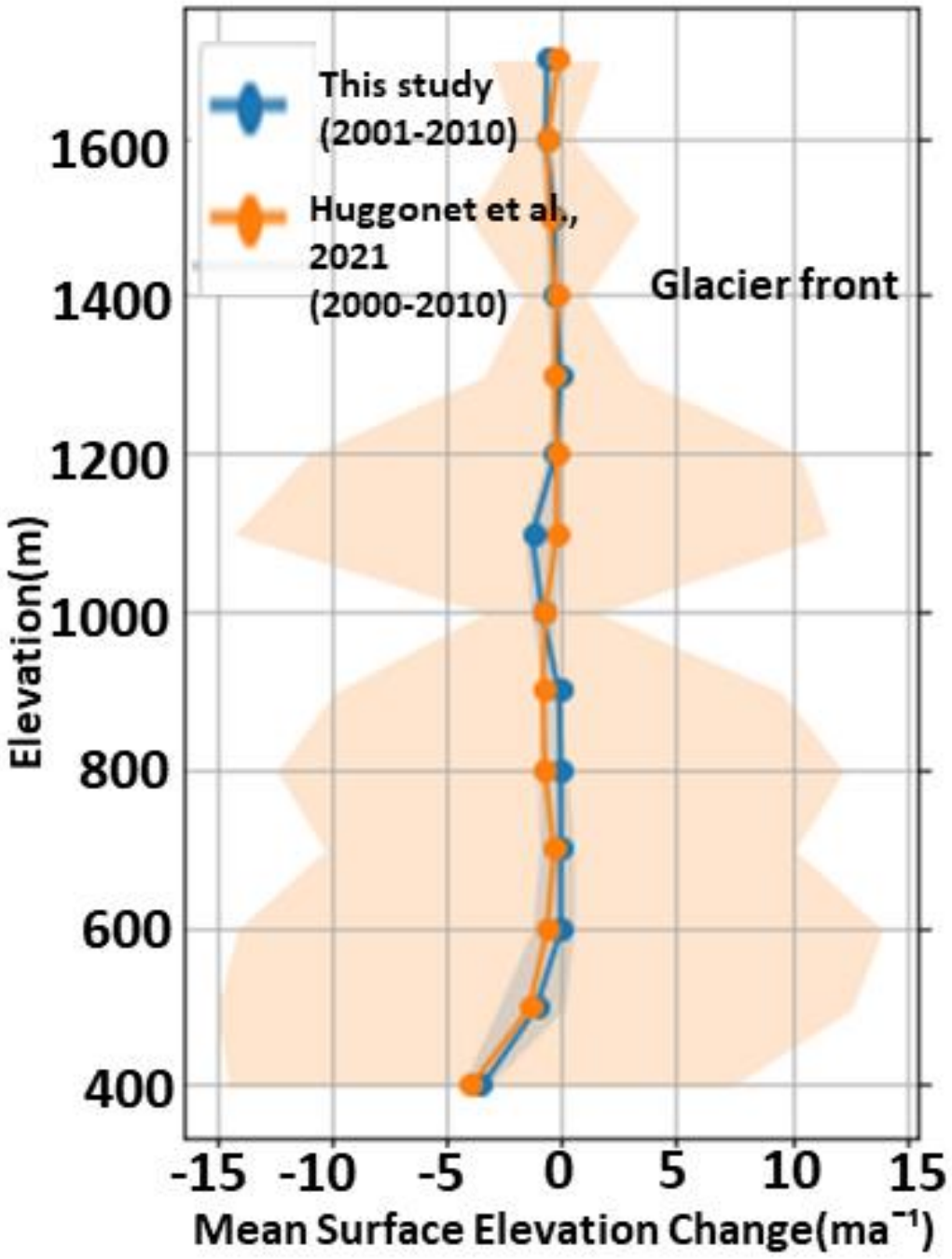


*Figure 6.4: Change in mean surface elevation per year per altitudinal band for the different 2001- 2010 for this study and 2000 -2010 Hugonnet et al.,2021. Shaded error bars represent the error for the studies.*

the frontal part of Briksdalbreen in this study. Nigardsbreen, Baklibreen and Bergsetsbreen thickened by a mean of 24.6 ± 5.1 m, 14.3 ± 5.1 m, 3.2 ± 5.1 m between 1993 - 2001 respectively while this study found average thickness 0.3 ± 0.08 m for Briksdalsbreen. Although these results cannot be directly compared because of the difference in the glacier area and geometry, the results show that the surface of Briksdalbreen did not change significantly relative to others. However, it advanced by ∼ 12m in each of this period. The steepness of the glacier likely facilitated a quick transport of ice move down the glacier valley thereby reducing thick accumulation on the glacier front. Similar reason was given by Wangensteen et al., 2006 for the relatively low value obtained for the surface elevation change (3.2 m) of Bergsetbreen between 1993 – 2001.

Changes of Norwegian glaciers based on field and remotes sensing observations (including LiDAR DEMs and contour maps derived from aerial photographs) on sample glaciers for a period of 1960 - 2018 was conducted by Andreassen et al.,2020. Their results show an average retreat of 564 m with a range of 5 – 1400 m for 30 glaciers for a period of 50 years. The trend in length change from this study align with those of some selected reference glaciers reported by Andreassen et al.,2020 (Figure 6.5). Generally, most glaciers advanced until the late 1990s before they started to retreat. Nigardsbreen, retreated more than twice (∼1200 m) the retreat of Briksdalbreen between 1966 – 2018 while Rembesdalkåka retreated only as much of Briksdalbreen within the same time interval. Based on Andreassen et al.,2020, it is tempting to conclude that Briksdalbeen retreated averagely (∼500 m) between 1966 - 2020 in context of the Norwagian glaciers, however the study does not cover all glaciers in Norway.

Whereas this study found a geodetic mass balance of of - 0.045 m w.e $a^{-1}$ for 1966-2020 and -0.25 m w.e $a^{-1}$ 2010-2020 for Briksdalsbreen, Andreassen et al., (2020) reported a geodetic mass balance of the - 0.27 m w.e $a^{-1}$ and -0.97 m w.e $a^{-1}$ between 1960 – 2018 and 2001 – 2010 respectively for a total of 131 Norwagian glaciers. The geodetic mass balance computed in this study showed mass deficit between 1960 and 2020 like the measured mass balance of most glaciers in southern Norway (Figure 6.5) and a higher negative mass balance in 2001 -2010 as observed Andreassen et al., (2020). However mass balance can vary for each glacier and cannot be accurately compared. For example, the observed mass balance of Nigardsbreen between 1962 – 2021 is positive (+0.06 m w.e $a^{-1}$)(Andreassen et al.,2022) contrary to the observation of many other glaciers. A clear regional pattern and gradient in mass balance are yet to be defined in southern Norway as

neighbouring glaciers show variability in mass balance Andreassen et al., (2020). Studies have shown that area, topography and surrounding feature such as lakes can create difference in the mass balance of glaciers in the same region. Hence, it is difficult to directly compare the mass balance of different glaciers without taking their geometry into account.

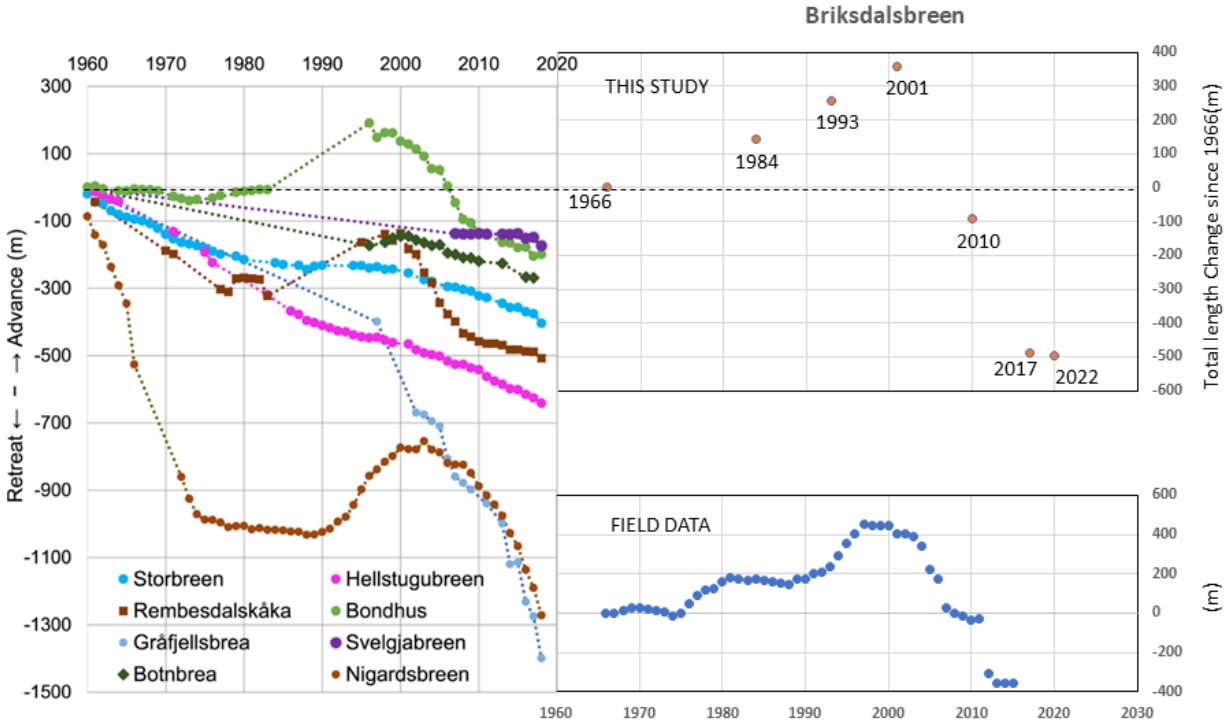


*Figure 6.5: Comparison of length changes of Briksdalbreen and other glaciers in western Norway. Dotted lines are used to connect discontinuous measurements (Modified from Andreassen et al.,*

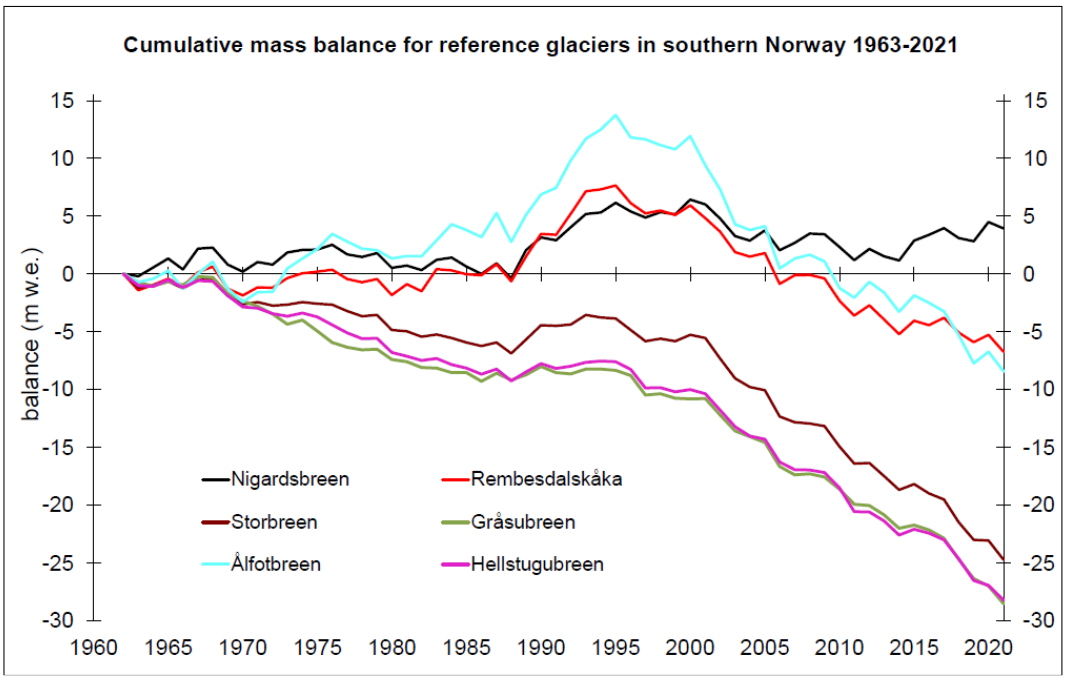


*Figure 6.6: Mass balance of reference Norwegian glaciers ( Andreassen et al., (2022)*

### 6.4 Climate and changes on Briksdalsbreen

Previous studies have found a good correlation between climate and observed changes in length of Briksdalsbreen between 1901 to 2004 (Nesje 1995, Nesje 2005) (Figure 6). The changes in Briksdalsbreen are controlled by winter precipitation and summer temperatures (Nesje 2005). In this study, the advance of the glacier front between 1966 – 2001 correlated well with increase precipitation (Figure 6.7) but the retreat from between 2001 – 2020 is related to high summer temparture. Winter precipitation (relative to the period 1900 – 2000 = 1030 m) increased from 1966 until 1992 with interannual variability (Figure 6.7). This increase account for the advance of Briksdalsbreen recorded in this study between 1966 – 1984 (144 m) and 1984 – 1993 (114 m). After 1992, winter precipitation reduced sharply until 2000 after increased at a very small rate. Therefore, the large retreat and negative mass balance of the glacier recorded during from 2001 upward can not be associated with winter precipitation. As show in Figure 6.9, summer temperature (relative to 1900 – 2000 = 12.78$^{o}$C) began to increase around 1989/1990 and has continued to increase with variation from year to year. Ablation caused by high summer temperature cause can explain the retreat recorded between 2001 – 2020.

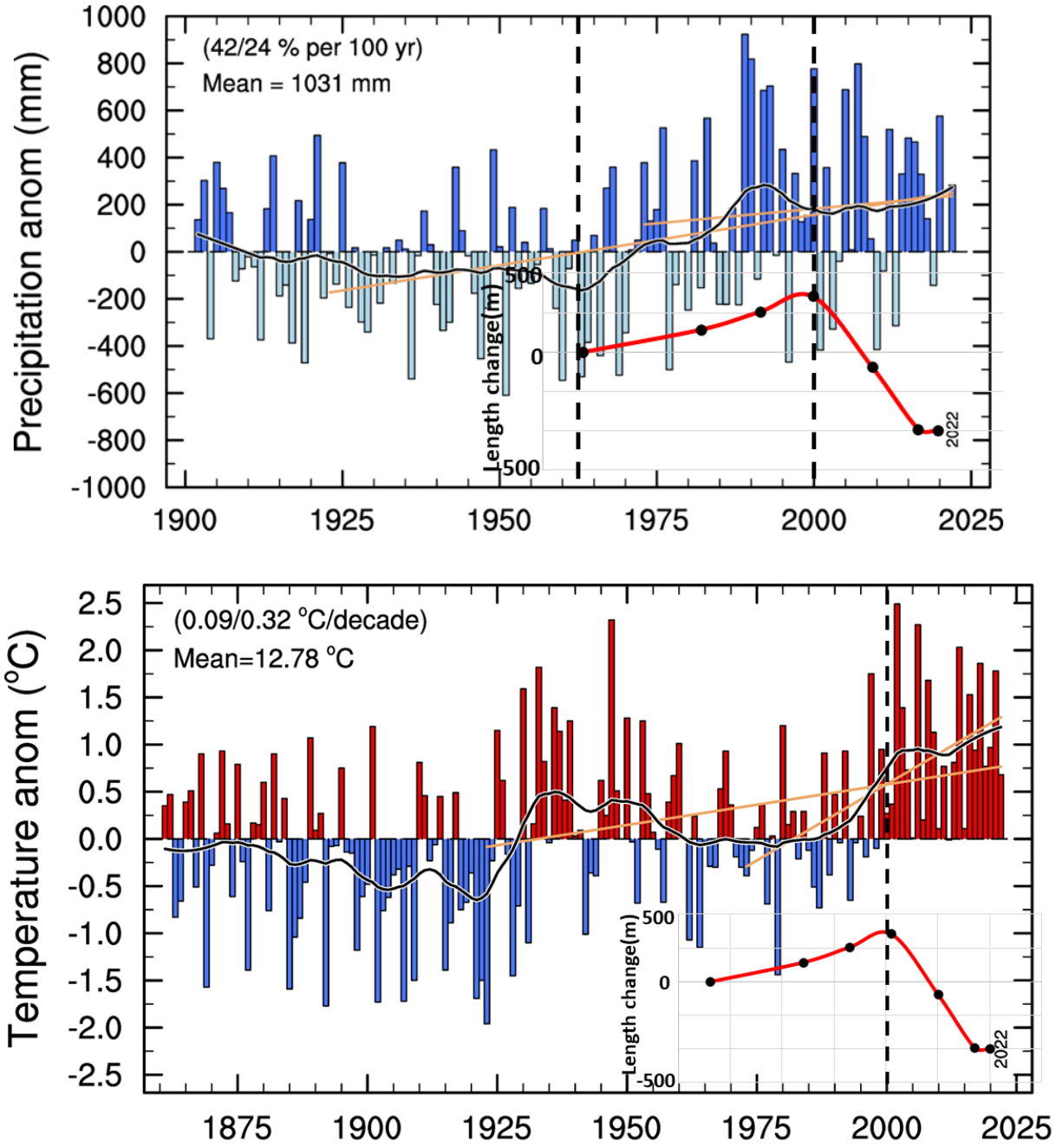


*Figure 6.7: Top- Summer temperature, Middle- winter precipitation Bottom-length changes on Brikdalsbreen. Observed change of annual mean precipitation for Norway since year 1900, relative to the 1901-2000 mean. The trend lines (grey colour) show the linear trends for the last 100 and 50 years. Temperature and precipitation data are from eKlima of Norwagian Meterological institute (downloaded from Helge Drange page: folk.uib.no/ngfhd/Climate/climate-pnor03.html)*

### 6.5 Uncertainties

A major source of uncertainty in the generation of DEM for this study is the method used in the acquisition of ground control points (GCP). The GCPs were collected from google earth with about 15m resolution, therefore, precise location of the positions is almost impossible. Moreover, a large fraction of study area of is covered by snow thus very few features are available and visible for selection as GCP. For this reason, the criteria of evenly distributed GCP were hardly met in this study as most GCPs were selected close to the glacier front where the surface is snow free and some feature can be easily identified. Although the co-registration process is expected to minimize biases associated with this shortcoming, the extent which this achieve cannot be accurately quantified. Even with high degree deramping, it impossible to eliminate non-linear biases in DEM.

The number of images used in optical photogrammetry can influence the quality of the DEM produced. Only few images were available in each set of aerial photographs used for this study. Each image set contains less than 8 images and, in most cases, less the 4 cover the area of interest. In some cases, such (for 1997 set) the images have no sufficient overlap for photogrammetric processing. Likewise, all set of aerial photographs used in this study contain shadows at either at the terminus or valley sides of the glaciers. This introduced erroneous surface elevation difference values on the glacier and the stable ground. Although attempts were made to filter some of these anomalies, a perfect adjustment was not achieved. It is likely that the elevation differences along terminus and the sides of the glacier are overestimated.

In addition, the crevassed zones on the glacier are clearly marked by values of spurious surface elevation difference values especially on outputs involving 2010, 2017 and 2020 images. It is difficult attribute this to error to true changes in the crevasses as most images show some shadow over the crevasses. Similarly, the 2017 DEM contains a small stripe zone of error along the southern boundary of the glacier, although filtering this zone does not affect the observed mean change in elevation significantly. Seasonal snow cover created ambiguity in the accurate identification of glaciers outlines. When updating glacier outlines with orthomosaic images, snow covers in 2001,1993 and 1984 presented challenges in locating the exact position of the glacier outlines. The author used his discretion to fit a glacier outline for these years as no method was found in literature to tackle the problem. Therefore, the glacier areas for this may either be overestimated or underestimated.

Regarding the method used in this study for quantifying error, it is robust and based on logical framework of spatial statistics (Huggonet *et al*, 2022), however it produced very low error values for this study compared to other studies.

# Chapter 7 : Conclusion

1. Changes in Briksdalsbreen between 1966 – 2020 were investigated in this study using multi-temporal aerial photographs, LiDAR-based Digital Elevation Model (DEM) and the glacier outline.

2. The study showed that Briksdalsbreen retreated ~ 450 m ( -8.4 m $a^{-1}$), shrunk by 0.04 % $a^{-1}$ and thinned by – 2. 98 m ( -0.06 m $a^{-1}$) in the 54 years (1966 – 2020). It lost mass of -0.045 ±0.05 m w. e. $a^{-1}$.

3. Within the period investigated in this study, the front of Briksdalsbreen advance from between 1966 - 2001 and retreated very fast from 2001 – 2020 with the highest recorded retreat between 2001 – 2010.

4. Climate data correlated with the measured length changes. High winter precipitations accounted for Briksdalsbreen advance in the 1990s while high summer temperature caused the observed retreat of the glacier in the 2000s.

5. The study agrees with field observations of changes in length of Briksdalsbreen and the result of a regional study covering Briksdalsbreen, unfortunately, there are no field measurement of mass balance to serve a comparative purpose for this study.

6. This result show that Remote sensing can provides useful information about glaciers changes.

## References


Åkesson, H., Nisancioglu, K. H., Giesen, R. H., & Morlighem, M. (2017). Simulating the evolution of Hardangerjøkulen ice cap in southern Norway since the mid-Holocene and its sensitivity to climate change. *The Cryosphere*, *11*(1), 281-302.

Andreassen, L. M., & Elvehøy, H. (2021). Norwegian Glacier Reference Dataset for Climate Change Studies.

Andreassen, L. M., Elvehøy, H., & Kjøllmoen, B. (2002). Using aerial photography to study glacier changes in Norway. *Annals of Glaciology*, *34*, 343-348.

Andreassen, L. M., Elvehøy, H., Kjøllmoen, B., & Belart, J. M. (2020). Glacier change in Norway since the 1960s–an overview of mass balance, area, length and surface elevation changes. *Journal of Glaciology*, *66*(256), 313-328.

Andreassen, L. M., Elvehøy, H., Kjøllmoen, B., Engeset, R. V., & Haakensen, N. (2005). Glacier mass-balance and length variation in Norway. *Annals of Glaciology*, *42*, 317-325.

Andreassen, L. M., Paul, F., Kääb, A., & Hausberg, J. E. (2008). Landsat-derived glacier inventory for Jotunheimen, Norway, and deduced glacier changes since the 1930s. *The Cryosphere*, *2*(2), 131-145.

Andreassen, L. M., Winsvold, S. H., Paul, F., & Hausberg, J. E. (2012). Inventory of Norwegian glaciers. *Rapport*, *38*.

Baumann, S., Anderson, B., Chinn, T., Mackintosh, A., Collier, C., Lorrey, A. M., ... & Eaves, S. (2021). Updated inventory of glacier ice in New Zealand based on 2016 satellite imagery. *Journal of glaciology*, *67*(261), 13-26.

Beniston, M., Farinotti, D., Stoffel, M., Andreassen, L. M., Coppola, E., Eckert, N., ... & Vincent, C. (2018). The European mountain cryosphere: a review of its current state, trends, and future challenges. *The Cryosphere*, *12*(2), 759-794.

Carrivick, J. L., Andreassen, L. M., Nesje, A., & Yde, J. C. (2022). A reconstruction of Jostedalsbreen during the Little Ice Age and geometric changes to outlet glaciers since then. *Quaternary Science Reviews*, *284*, 107501.

Cuffey, K. M., & Paterson, W. S. B. (2010). *The physics of glaciers*. Academic Press.

Cunde, X., Shijin, W., & Dahe, Q. (2016). A preliminary study on cryosphere service function and its value estimation. *Advances in Climate Change Research*, *12*(1), 45.

Edwards, T. L., Nowicki, S., Marzeion, B., Hock, R., Goelzer, H., Seroussi, H., ... & Zwinger, T. (2021). Projected land ice contributions to twenty-first-century sea level rise. *Nature*, *593*(7857), 74-82.

Farinotti, D., Huss, M., Fürst, J. J., Landmann, J., Machguth, H., Maussion, F., & Pandit, A. (2019). A consensus estimates for the ice thickness distribution of all glaciers on Earth. *Nature Geoscience*, *12*(3), 168-173.

Gleick, P. H. (1998). Water in crisis: paths to sustainable water use. *Ecological applications*, *8*(3), 571-579.

Grove, J. M. (2004). *Little ice ages: ancient and modern* (Vol. 1). Taylor & Francis.

Gudmundsson, S., Björnsson, H., Magnusson, E., Berthier, E., Palsson, F., Gudmundsson, M. T., ... & Dall, J. (2011). Response of Eyjafjallajökull, Torfajökull and Tindfjallajökull ice caps in Iceland to regional warming, deduced by remote sensing. *Polar Research*, *30*(1), 7282.

Haeberli, W., & Beniston, M. (1998). Climate change and its impacts on glaciers and permafrost in the Alps. *Ambio*, 258-265.

Haeberli, W., Kääb, A., Mühll, D. V., & Teysseire, P. (2001). Prevention of outburst floods from periglacial lakes at Grubengletscher, Valais, Swiss Alps. *Journal of Glaciology*, *47*(156), 111-122.

Hiemstra, J. F., Young, G. H., Loader, N. J., & Gordon, P. R. (2022). Interrogating glacier mass balance response to climatic change since the Little Ice Age: reconstructions for the Jotunheimen region, southern Norway. *Boreas*, *51*(2), 350-363.

Hoeser, T., & Kuenzer, C. (2020). Object detection and image segmentation with deep learning on earth observation data: A review-part i: Evolution and recent trends. *Remote Sensing*, *12*(10), 1667.

Hugonnet, R., Brun, F., Berthier, E., Dehecq, A., Mannerfelt, E. S., Eckert, N., & Farinotti, D. (2022). Uncertainty analysis of digital elevation models by spatial inference from stable terrain. *IEEE Journal of Selected Topics in Applied Earth Observations and Remote Sensing*, *15*, 6456-6472.

Hugonnet, R., McNabb, R., Berthier, E., Menounos, B., Nuth, C., Girod, L., ... & Kääb, A. (2021). Accelerated global glacier mass loss in the early twenty-first century. *Nature*, *592*(7856), 726-731.

Hugonnet, R., McNabb, R., Berthier, E., Menounos, B., Nuth, C., Girod, L., ... & Kääb, A. (2021). Accelerated global glacier mass loss in the early twenty-first century. *Nature*, *592*(7856), 726-731.

Hurrell, J. W., Kushnir, Y., Ottersen, G., & Visbeck, M. (2003). An overview of the North Atlantic oscillation. *Geophysical Monograph-American Geophysical Union*, *134*, 1-36.

Imhof, P., Nesje, A., & Nussbaumer, S. U. (2012). Climate and glacier fluctuations at Jostedalsbreen and Folgefonna, southwestern Norway and in the western Alps from the 'Little Ice Age'until the present: The influence of the North Atlantic Oscillation. *The Holocene*, *22*(2), 235-247.

IPCC 2019: Hock, R., Rasul, G., Adler, C., Cáceres, B., Gruber, S., Hirabayashi, Y., ... & Zhang, Y. (2019). High mountain areas. In *IPCC special report on the ocean and cryosphere in a changing climate* (pp. 131-202). H.-O. Pörtner, DC Roberts, V. Masson-Delmotte, P. Zhai, M. Tignor, E. Poloczanska, K. Mintenbeck, A. Alegría, M. Nicolai, A. Okem, J. Petzold, B. Rama, NM Weyer (eds.).

IPCC 2021: Allan, R. P., Hawkins, E., Bellouin, N., & Collins, B. (2021). IPCC, 2021: summary for Policymakers.

IPCC: Field, C. B., Barros, V., Stocker, T. F., & Dahe, Q. (Eds.). (2012). *Managing the risks of extreme events and disasters to advance climate change adaptation: special report of the intergovernmental panel on climate change*. Cambridge University Press.

Jaggard, K. W., Qi, A., & Ober, E. S. (2010). Possible changes to arable crop yields by 2050. *Philosophical Transactions of the Royal Society B: Biological Sciences*, *365*(1554), 2835-2851.

Kääb, A. (2002). Monitoring high-mountain terrain deformation from repeated air-and spaceborne optical data: examples using digital aerial imagery and ASTER data. *ISPRS Journal of Photogrammetry and remote sensing*, *57*(1-2), 39-52.

Kääb, A., Huggel, C., Fischer, L., Guex, S., Paul, F., Roer, I., ... & Weidmann, Y. (2005b). Remote sensing of glacier-and permafrost-related hazards in high mountains: an overview. *Natural Hazards and Earth System Sciences*, *5*(4), 527-554.

Kääb, Andreas, Tobias Bolch, Kimberly Casey, Torborg Heid, Jeffrey S. Kargel, Gregory J. Leonard, Frank Paul, and Bruce H. Raup. "Glacier mapping and monitoring using multispectral data." *Global land ice measurements from space* (2014): 75-112.

König, M., Winther, J. G., & Isaksson, E. (2001). Measuring snow and glacier ice properties from satellite. *Reviews of Geophysics*, *39*(1), 1-27.

Kumar, A., Schei, T., Ahenkorah, A., Rodriguez, R. C., Devernay, J. M., Freitas, M., ... & Liu, Z. (2011). Hydropower IPCC Special Report on Renewable Energy Sources and Climate Change Mitigation. *Cambridge University Press, Cambridge, United Kingdom and New York, NY, USA*.

Laumann, T., & Nesje, A. (2009). The impact of climate change on future frontal variations of Briksdalsbreen, western Norway. *Journal of Glaciology*, *55*(193), 789-796.

Melvold, K., Laumann, T., & Nesje, A. (2011). Kupert landskap under Hardangerjøkulen. *Norge: GEO. Tilgjengelig fra: http://www. geoforskning. no/reportasjene/38-kupert-landskap-under-hardangerjokulen [Accessed 29.11. 2014 2014]*.

Nesje, A. (2005). Briksdalsbreen in western Norway: AD 1900-2004 frontal fluctuations as a combined effect of variations in winter precipitation and summer temperature. *The Holocene*, *15*(8), 1245-1252.

Nesje, A., & Matthews, J. A. (2012). The Briksdalsbre Event: A winter precipitation-induced decadal-scale glacial advance in southern Norway in the ad 1990s and its implications. *The Holocene*, *22*(2), 249-261.

Nesje, A., Dahl, S. O., Thun, T., & Nordli, Ø. (2008). The 'Little Ice Age'glacial expansion in western Scandinavia: summer temperature or winter precipitation?. *Climate dynamics*, *30*, 789-801.

Nesje, A., Johannessen, T., & Birks, H. J. B. (1995). Briksdalsbreen, western Norway: climatic effects on the terminal response of a temperate glacier between AD 1901 and 1994. *The Holocene*, *5*(3), 343-347.

Nuth, C., & Kääb, A. (2011). Co-registration and bias corrections of satellite elevation data sets for quantifying glacier thickness change. *The Cryosphere*, *5*(1), 271-290.

Paul, F., Bolch, T., Kääb, A., Nagler, T., Nuth, C., Scharrer, K., ... & Van Niel, T. (2015). The glaciers climate change initiative: Methods for creating glacier area, elevation change and velocity products. *Remote Sensing of Environment*, *162*, 408-426.

Paul, F., Bolch, T., Kääb, A., Nagler, T., Nuth, C., Scharrer, K., ... & Van Niel, T. (2015). The glaciers climate change initiative: Methods for creating glacier area, elevation change and velocity products. *Remote Sensing of Environment*, *162*, 408-426.

Pfeffer, W. T., Arendt, A. A., Bliss, A., Bolch, T., Cogley, J. G., Gardner, A. S., ... & Randolph Consortium. (2014). The Randolph Glacier Inventory: a globally complete inventory of glaciers. *Journal of glaciology*, *60*(221), 537-552.

Post, A., & LaChapelle, E. R. (2000). *Glacier ice*. University of Toronto Press.

Racoviteanu, A. E., Williams, M. W., & Barry, R. G. (2008). Optical remote sensing of glacier characteristics: a review with focus on the Himalaya. *Sensors*, *8*(5), 3355-3383.

Robson, B. A. (2012). *A Remote Sensing Investigation into the evolution of Folgefonna Glacier over the last 150 years* (Master's thesis, The University of Bergen).

Robson, B. A., MacDonell, S., Ayala, Á., Bolch, T., Nielsen, P. R., & Vivero, S. (2022). Glacier and rock glacier changes since the 1950s in the La Laguna catchment, Chile. *The Cryosphere*, *16*(2), 647-665.

Robson, B. A., Nuth, C., Dahl, S. O., Hölbling, D., Strozzi, T., & Nielsen, P. R. (2015). Automated classification of debris-covered glaciers combining optical, SAR and topographic data in an object-based environment. *Remote Sensing of Environment*, *170*, 372-387.

Rose, K. C., Hart, J. K., & Martinez, K. (2009). Seasonal changes in basal conditions at Briksdalsbreen, Norway: the winter–spring transition. *Boreas*, *38*(3), 579-590.

Steiger, R. (2010). The impact of climate change on ski season length and snowmaking requirements in Tyrol, Austria. *Climate research*, *43*(3), 251-262.

Taylor, L. S., Quincey, D. J., Smith, M. W., Baumhoer, C. A., McMillan, M., & Mansell, D. T. (2021). Remote sensing of the mountain cryosphere: Current capabilities and future opportunities for research. *Progress in Physical Geography: Earth and Environment*, *45*(6), 931-964.

Taylor, L. S., Quincey, D. J., Smith, M. W., Baumhoer, C. A., McMillan, M., & Mansell, D. T. (2021). Remote sensing of the mountain cryosphere: Current capabilities and future opportunities for research. *Progress in Physical Geography: Earth and Environment*, *45*(6), 931-964.

Vaughan, D. G., Comiso, J. C., Allison, I., Carrasco, J., Kaser, G., Kwok, R., ... & Zhang, T. (2013). Observations: cryosphere. *Climate change*, *2103*, 317-382.

Vivero, S., Bodin, X., Farías-Barahona, D., MacDonell, S., Schaffer, N., Robson, B. A., & Lambiel, C. (2021). Combination of aerial, satellite, and UAV photogrammetry for quantifying rock glacier kinematics in the dry Andes of Chile (30 S) since the 1950s. *Frontiers in Remote Sensing*, *2*, 784015.

Wangensteen, B., Tønsberg, O. M., Kääb, A., Eiken, T., & Hagen, J. O. (2006). Surface elevation change and high resolution surface velocities for advancing outlets of Jostedalsbreen. *Geografiska Annaler: Series A, Physical Geography*, *88*(1), 55-74.

Way, Robert G., Trevor Bell, and Nicholas E. Barrand. "An inventory and topographic analysis of glaciers in the Torngat Mountains, northern Labrador, Canada." *Journal of Glaciology* 60, no. 223 (2014): 945-956

WGMS (2016). Glacier Thickness Database 2.0.

Zemp, M., Huss, M., Thibert, E., Eckert, N., McNabb, R., Huber, J., ... & Cogley, J. G. (2019). Global glacier mass changes and their contributions to sea-level rise from 1961 to 2016. *Nature*, *568*(7752), 382-386.

Zhang, J., Jia, L., Menenti, M., & Hu, G. (2019). Glacier facies mapping using a machine-learning algorithm: The Parlung Zangbo Basin case study. *Remote Sensing*, *11*(4), 452.

Zhu, X. X., Tuia, D., Mou, L., Xia, G. S., Zhang, L., Xu, F., & Fraundorfer, F. (2017). Deep learning in remote sensing: A comprehensive review and list of resources. *IEEE geoscience and remote sensing magazine*, *5*(4), 8-36.